AD-A173 400 THE CHARACTERIZATION OF OFF VERTICAL RETURN ERROR IN FREE-SURFACE MEASURE..(U) DAVID W TAYLOR NAVAL SHIP RESEARCH AND DEVELOPMENT CENTER BET.. R D PIERCE 1/1

UNCLASSIFIED SEP 86 DTNSRDC-86/060 F/G 20/1 NL

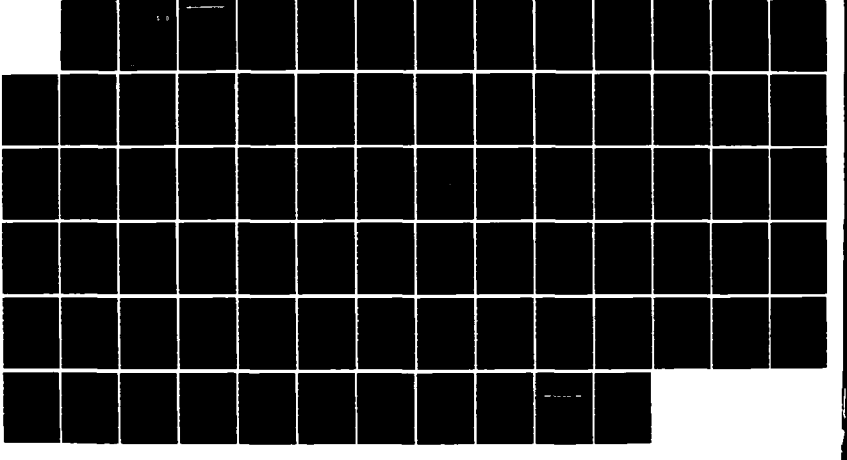

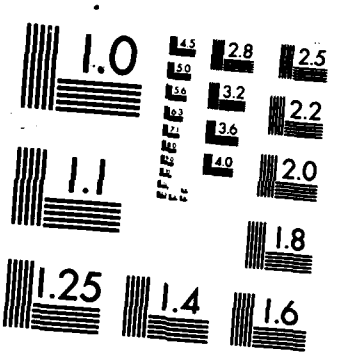

David W. Taylor Naval Ship Research and Development Center
Bethesda, MD 20084-5000

DTNSRDC-86/060 September 1986

Central Instrumentation Department
Research and Development Report

The Characterization of Off Vertical Return Error in Free-Surface Measurements by Ultrasonic Displacement Sensors

by
Robert Dorrington Pierce

DTNSRDC-86/060 The Characterization of Off Vertical Return Error in Free-Surface Measurements by Ultrasonic Displacement Sensors

MAJOR DTNSRDC TECHNICAL COMPONENTS

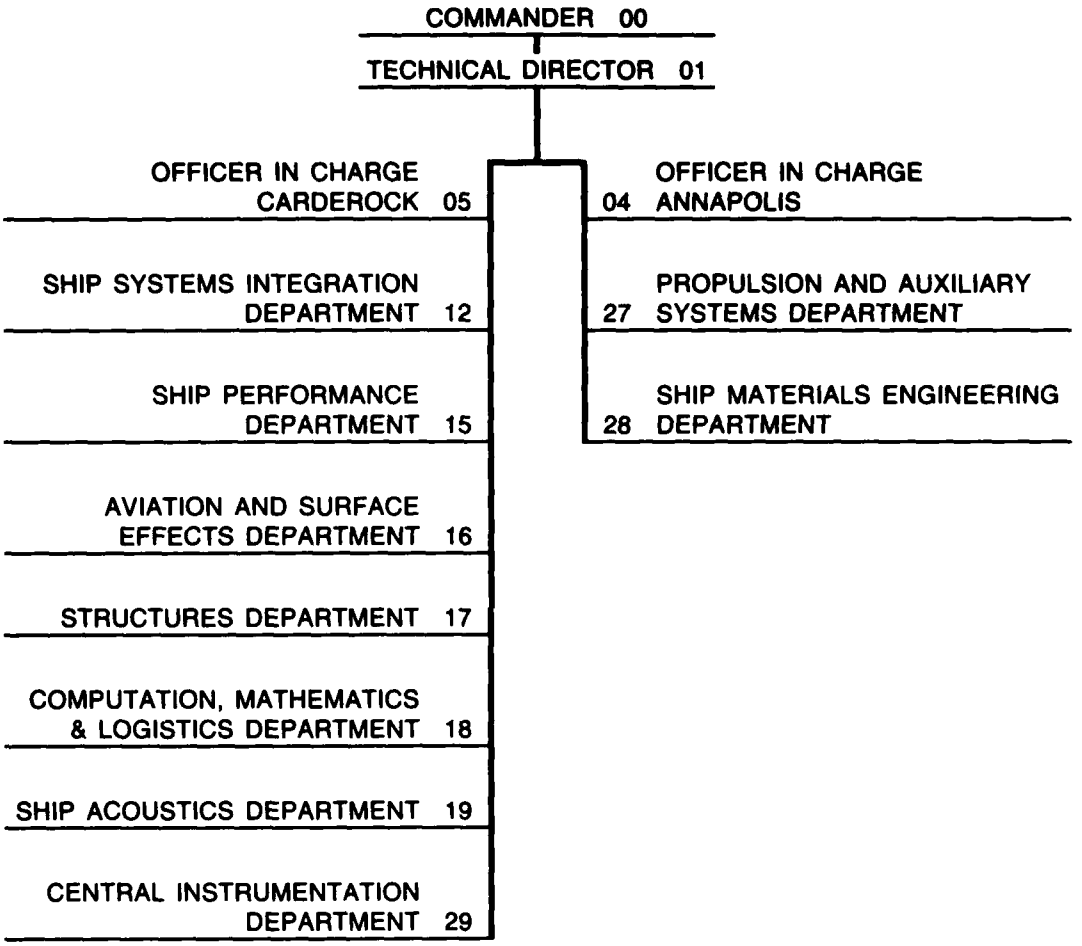

DESTRUCTION NOTICE — For **classified** documents, follow the procedures in DOD 5220.22M, Industrial Security Manual, Section II-9, or DOD 5200.1-R, Information Security Program Regulation, Chapter IX. For **unclassified**, limited documents, destroy by any method that will prevent disclosure of contents or reconstruction of the document.

UNCLASSIFIED
SECURITY CLASSIFICATION OF THIS PAGE

REPORT DOCUMENTATION PAGE

1a REPORT SECURITY CLASSIFICATION UNCLASSIFIED	1b RESTRICTIVE MARKINGS AD-A173 400
2a SECURITY CLASSIFICATION AUTHORITY	3 DISTRIBUTION / AVAILABILITY OF REPORT APPROVED FOR PUBLIC RELEASE; DISTRIBUTION IS UNLIMITED.
2b DECLASSIFICATION / DOWNGRADING SCHEDULE	
4 PERFORMING ORGANIZATION REPORT NUMBER(S) DTNSRDC-86/060	5 MONITORING ORGANIZATION REPORT NUMBER(S)
6a NAME OF PERFORMING ORGANIZATION David W. Taylor Naval Ship R&D Center	6b OFFICE SYMBOL (If applicable) Code 2960
6c ADDRESS (City, State, and ZIP Code) Bethesda, Maryland 20084-5000	7a NAME OF MONITORING ORGANIZATION 7b ADDRESS (City, State, and ZIP Code)
8a NAME OF FUNDING / SPONSORING ORGANIZATION	8b OFFICE SYMBOL (If applicable)
8c ADDRESS (City, State, and ZIP Code)	9 PROCUREMENT INSTRUMENT IDENTIFICATION NUMBER

10 SOURCE OF FUNDING NUMBERS			
PROGRAM ELEMENT NO	PROJECT NO	TASK NO	WORK UNIT ACCESSION NO
None	None	None	None

11 TITLE (Include Security Classification)
THE CHARACTERIZATION OF OFF VERTICAL RETURN ERROR IN FREE-SURFACE MEASUREMENTS BY ULTRASONIC DISPLACEMENT SENSORS

12 PERSONAL AUTHOR(S)
Pierce, Robert Dorrington

13a TYPE OF REPORT	13b TIME COVERED	14 DATE OF REPORT (Year, Month, Day)	15 PAGE COUNT
Final	FROM TO	1986 September	78

16 SUPPLEMENTARY NOTATION
A thesis submitted to the faculty of the School of Engineering and Applied Science, Department of Civil, Mechanical and Environmental Engineering of the George (continued)

17 COSATI CODES			18 SUBJECT TERMS (Continue on reverse if necessary and identify by block number)	
FIELD	GROUP	SUB-GROUP	Sensors	Wave Height
			Ultrasonic	Order Analysis
			Displacement	Simulation

19 ABSTRACT (Continue on reverse if necessary and identify by block number)

Ultrasonic displacement sensors are used to measure the free surface elevation of water waves (wave height). These sensors emit a sound burst that echos off the water surface; the time between transmitting the burst and receiving an echo is converted into a measurement of distance. Since echos are received from surface regions that are offset from vertical, these displacement measurements contain off vertical return error. The characteristics of this error source are determined by the development of an analytical model of this effect. This model is verified using computer simulations with sinusoidal and random wave profiles. A limited set of experimentally obtained results are compared to this analytical model. The results obtained from this model include the linear transfer function between actual and measured wave height, the mean value shift in the measured wave height, the echo return angle, and for sinusoidal wave profiles, the second harmonic amplitude in the measured wave height. These results describe the effect this error has on wave

(continued)

20 DISTRIBUTION / AVAILABILITY OF ABSTRACT	21 ABSTRACT SECURITY CLASSIFICATION	
☒ UNCLASSIFIED UNLIMITED ☐ SAME AS RPT ☐ DTIC USERS	UNCLASSIFIED	
22a NAME OF RESPONSIBLE INDIVIDUAL Robert D. Pierce	22b TELEPHONE (Include Area Code) (202) 227-1591	22c OFFICE SYMBOL Code 2960

DD FORM 1473, 84 MAR 83 APR edition may be used until exhausted
All other editions are obsolete

SECURITY CLASSIFICATION OF THIS PAGE
UNCLASSIFIED

(Block 16 continued)

Washington University in partial satisfaction of the requirements for the degree of Master of Science in Ocean and Marine Engineering (Dec 1981). Thesis directed by Dr. David D. Moran, Professional Lecturer.

(Block 19 continued)

height measurements. Except for the echo return angle, the magnitude of these effects are dependent on the height of the sensor above the undisturbed free surface, so the degree of error is controllable. The mean value shift provides a method of measuring wave slope that is independent of a wave dispersion relationship. Since the ultrasonic transducers that are used by this measurement system operate over a limited beamwidth, the echo return angle results aid in selecting these transducers.

TABLE OF CONTENTS

TABLE OF CONTENTS (Continued)

LIST OF FIGURES

LIST OF FIGURES (Continued)

Page

LIST OF TABLES

NOTATION

A	Single amplitude wave height of sinusoidal wave profile
A_2	Second harmonic of measured wave height for sinusoidal wave profile
D	Vertical distance from sonic sensor to wave profile
D_m	Distance from sonic sensor to closest point on wave profile
$E[\cdot]$	Expectation operator
f	Actual wave profile
f_x	First spatial derivative of actual wave profile
f_{xx}	Second spatial derivative of actual wave profile
f_m	Measured wave profile
g	Gravitational constant
$H(\omega)$	Linear transfer function
i	Imaginary number, square root of -1
k	Wave number
$O(\cdot)$	Order of magnitude operator
R_c	Radius of curvature
$R(\Delta x)$	Remainder in root search operation
$R_{ff}(\tau)$	Auto correlation of actual wave profile
$R_{f_m f_m}(\tau)$	Auto correlation of measured wave profile
$R_{ff_m}(\tau)$	Cross correlation between actual and measured wave profile
$R_{ff_{xx}}(\tau)$	Cross correlation between actual wave profile and its second spatial derivative
$R_{f_x f_x}(\tau)$	Auto correlation of wave slope

NOTATION (continued)

$S_{ff}(\omega)$	Auto spectrum of actual wave profile
$S_{f_m f_m}(\omega)$	Auto spectrum of measured wave profile
$S_{ff_m}(\omega)$	Cross spectrum of actual and measured wave profile
$S_{ff_{xx}}(\omega)$	Cross spectrum of actual wave profile and its second spatial derivative
$S_{f_x f_x}(\omega)$	Auto spectrum of the wave slope
$S_{f_{xx} f_{xx}}(\omega)$	Auto spectrum of the second derivative of the actual wave profile
t	Time
x	Horizontal distance
x_o	Horizontal location of sonic sensor
Δx	Horizontal location of the return echo relative to the sonic sensor
y	Vertical distance
Y	Height of the sonic sensor above the undisturbed water surface
$\gamma^2(\omega)$	Coherency
ε	Wave slope parameter used in order of magnitude analysis
θ	Angle of the returned sonic echo relative to vertical
θ_p	Peak angle of the returned sonic echo for the sinusoidal wave profile
λ	Wave length
μ_{f_m}	Mean value of measured wave height
σ_f^2	Variance of actual wave height
$\sigma_{f_m}^2$	Variance of measured wave height
$\sigma_{f_x}^2$	Variance of wave slope

NOTATION (continued)

$\sigma^2_{f_{xx}}$	Variance of wave profiles second spatial derivative
σ^2_{θ}	Variance of the echo return angle for random wave profiles
τ	Time shift
Ψ	Phase of sinusoidal wave profile
ω	Frequency in radians per second
*	Complex conjugate

ABSTRACT

Ultrasonic displacement sensors are used to measure the free surface elevation of water waves (wave height). These sensors emit a sound burst that echos off the water surface; the time between transmitting the burst and receiving an echo is converted into a measurement of distance. Since echos are received from surface regions that are offset from vertical, these displacement measurements contain off vertical return error. The characteristics of this error source are determined by the development of an analytical model of this effect. This model is verified using computer simulations with sinusoidal and random wave profiles. A limited set of experimentally obtained results are compared to this analytical model. The results obtained from this model include the linear transfer function between actual and measured wave height, the mean value shift in the measured wave height, the echo return angle, and for sinusoidal wave profiles, the second harmonic amplitude in the measured wave height. These results describe the effect this error has on wave height measurements. Except for the echo return angle, the magnitude of these effects are dependent on the height of the sensor above the undisturbed free surface, so the degree of error is controllable. The mean value shift provides a method of measuring wave slope that is independent of a wave dispersion relationship. Since the ultrasonic transducers that are used by this measurement system operate over a limited beamwidth, the echo return angle results aid in selecting these transducers.

1. INTRODUCTION

The free surface elevation of water waves can be measured using ultrasonic displacement sensors. Without contacting or disturbing the water surface, these sensors can measure the wave height in front of a test model that is traveling at high speeds. This method of measurement has desirable features, but it is also subject to various errors. One aspect of this measurement error that has not been investigated is the off vertical return error.

Off vertical return error exists because the ultrasonic displacement sensor gauges distance by emitting a sound burst that echos off the water surface. The echos that return to the sensor can originate from many points on this surface. The first detected echo determines the measured distance, and the surface region closest to the sensor will likely produce this detected echo. This echo, however, will rarely propagate from a surface region directly beneath the sensor. As the water wave propagates beneath the sensor, the surface region that produces the detected echo also varies. The actual wave height is the vertical distance from the

sensor to the wave, so the echos returned to the sensor from a surface region that is offset from vertical will define a measured distance that contains the off vertical return error.

The characteristics of the off vertical return error require definition. In planning an experiment that requires the use of an ultrasonic displacement sensor, two questions are raised: What controls exist which reduce the effects of the error, and, when analyzing the data from an experiment, what does this error do to the results? When designing experimental measurement techniques, another question is raised: Can any of these error characteristics be used to measure parameters of the water wave? An analytical model of this physical phenomena is developed to answer these questions.

The off vertical return error is a nonlinear phenomena, so its error characteristics depend on the wave profile being measured, and the analytical model is derived using expansions taken to a finite order. To verify this model, two different wave profiles are examined: regular waves (sinusoidal profile) and irregular waves (random profile). Various results, such as the transfer function between actual and measured wave height, are predicted by the analytical model. Next, from computer simulations performed using these profiles, the wave characteristics are compared to the results from the analytical model. The closeness of these results determine the regions where the analytical model is applicable. A limited set of experimentally obtained results are also compared to the analytical model.

The results that are compared for both sinusoidal and random wave profiles include those results that are common to either profile, such as the mean bias (mean value shift) and the linear transfer function between measured and actual wave height. Results specific to the sinusoidal wave profile are the second harmonic amplitude and maximum echo return angle. For the random wave profile, the specific results are the measured wave height auto spectrum and standard deviation, coherency, and the standard deviation of the echo return angle.

The linear transfer function has primary value in experiments and provides a direct measure of the reduction in amplitude incurred due to use of an ultrasonic displacement sensor. Mean bias has value as a method of measuring wave slope independent of a wave dispersion relationship. Since harmonics of the model motion and wave height are generally measured during regular wave experiments, the second harmonic amplitude provides information about the nonfundamental content of the measured wave height data that is due only to sensor operation. In the case of the

random wave profile, the auto spectrum, standard deviation and coherency results are extensions of the linear transfer function. Since the sonic transducers operate over a limited beamwidth, the maximum expected echo return angle and the standard deviation of the echo return angle have value in selecting these transducers. These results are generally parameterized by the sensor height to wave length ratio, so the error can be controlled by proper selection of the sensor's location above the undisturbed water level.

2. BACKGROUND AND ASSUMPTIONS

Ultrasonic displacement sensors are typically used at the David W. Taylor Naval Ship Research and Development Center (DTNSRDC) for wave height measurements in model testing and occasionally in full scale trials. In model basins, regular wave (sinusoidal profile) and irregular wave (random profile) experiments are performed. These ultrasonic sensors are mounted on the carriage, forward of the model, where the measured wave height is the forcing function to which the model is subjected. When mounted on the model, relative displacement measurements between the model and the waves are obtained. The principal advantage of these sensors is that the measurement is made without contacting or disturbing the water surface; encountered wave height measurements at high model speeds are obtained without the complication of moving a surface piercing sensor through the water.

The advantages of this type of wave height measurement device are great; however, major problems exist with these sensors. These sensors emit a sound burst and then listen for the return echo. The first returned echo that has an intensity greater than the sensor's detection threshold is detected, and the time delay between transmitting the burst and receiving this echo is converted into a measurement of displacement. When the returned echos do not exceed this detection threshold, a "drop out" occurs. If a multiple reflection from a previous sound burst (or noise) exceeds this threshold prior to a legitimate returned echo, then a "drop in" occurs. A discussion of these problems is given by Holton.[1*] The third major problem associated with these devices is that the received echo does not necessarily come from a point on the water surface that is directly beneath the sensor. This is the off vertical return error.

The analysis of the off vertical return error requires several assumptions. In general, these assumptions are made to isolate the off vertical return error problem;

*A complete listing of references is given on page 55.

however, some of these assumptions are necessary to make the analytical development of this error tractable. These assumptions fall into three categories: the acoustic medium, the ultrasonic displacement measurement system, and the wave profile.

The acoustic medium is air. Since the acoustic impedance of water is much greater than that of the air, very little sound energy will propagate into the water; the water profile is the only boundary seen by the acoustic wave. The air is assumed to be homogeneous and isotropic; the speed of sound is constant in this medium.

The ultrasonic displacement measurement system used at DTNSRDC is a Western Marine Electronics model LM4000 Prevision Level Monitor; however, the basic characteristics of this system are found in other commercial units. These devices use transducers that transmit and receive sound only over a limited beamwidth (+15 to -15 degrees, for example). The assumption is made that the beamwidth is unrestricted (+90 to -90 degrees); a return echo is therefore always possible. These devices only detect echos that have an intensity greater than the detection threshold. Here the assumption is made that the first received echo is detected. Since the first echo takes the shortest path, this assumption is reasonable. Most ultrasonic displacement sensors use a very high acoustical frequency (200 kilohertz, for example); however, the wave length of the sound in this acoustic pulse is finite so some distance ambiguity exists. Perfect measurements of displacement, however, are assumed. These devices transmit sound bursts periodically (60 times a second, for example), so the surface profile is sampled over a finite time. The assumption is made that the profile is frozen during each sample.

The wave profile is assumed to be unidirectional (two dimensional profile). High frequency wave clutter (background noise) will generally not fit this assumption. Breaking waves and spray are not considered. For the irregular wave conditions, these profiles are assumed to be Gaussian distributed in wave amplitude with zero mean. The assumption is made that these waves obey the deep water wave dispersion relationship given by linear wave theory.

For any of the wave profile conditions, several assumptions are made about the interaction of the acoustic wave with the water wave profile. Specular or mirror like reflection of the acoustic wave from the water profile is assumed. The acoustic wave length is assumed to be much smaller than the variations or wave lengths present in the water wave profile. The possibility of destructive interference that would cause an echo to pass undetected is not allowed.

The point on the profile directly beneath the sensor will often not produce the received echo; however, as the profile is examined further away from this centerline, the first point that can produce a received echo will be found. This point will likely produce the first received echo, but situations can be contrived such that some point further away in the horizontal direction will be the closest point to the sensor. For the analytical derivations, the point closest to this centerline is assumed to produce the first echo.

3. ANALYTICAL MODEL FOR THE OFF VERTICAL RETURN ERROR

The operation of the ultrasonic displacement sensor is viewed as a nonlinear physical system where the input is a given surface profile and the output is a distorted measure of this profile. This distortion is due to the off vertical return error; the returned sonic echo does not return from directly beneath the sensor. Since this system is nonlinear, the error or distortion is characterized for each specific input condition. For most model tests, two types of wave profiles are commonly used: regular waves where the profile is sinusoidal in shape and random waves where the profile is generally assumed to be Gaussian distributed. In this section, a mathematical model is derived for this off vertical return error; this model is then applied to characterize this error for these wave profiles.

3.1 OFF VERTICAL RETURN ECHOS

Since the acoustic wavelengths in the sound burst are assumed to be much smaller than the variations in the surface profile and specular reflections from the water profile are assumed, the echos received by the sensor will originate from those points on the profile that have an outward normal directed toward the sensor. These points on the profile are also at maximum and minimum distances from the sensor. The point on the wave profile from which the first returned echo originates has two characteristics: (1) A line drawn from the sensor to this point on the profile is perpendicular to the profile, and (2) This point on the profile is the shortest distance from the sensor to any other point on the profile.

These results are now proved by demonstrating that the same solution is obtained for either characteristic. The geometry is given in Figure 1, the wave profile is f(x).

The first requirement is to find solutions for Δx that minimize the distance D_m. D_m is given by

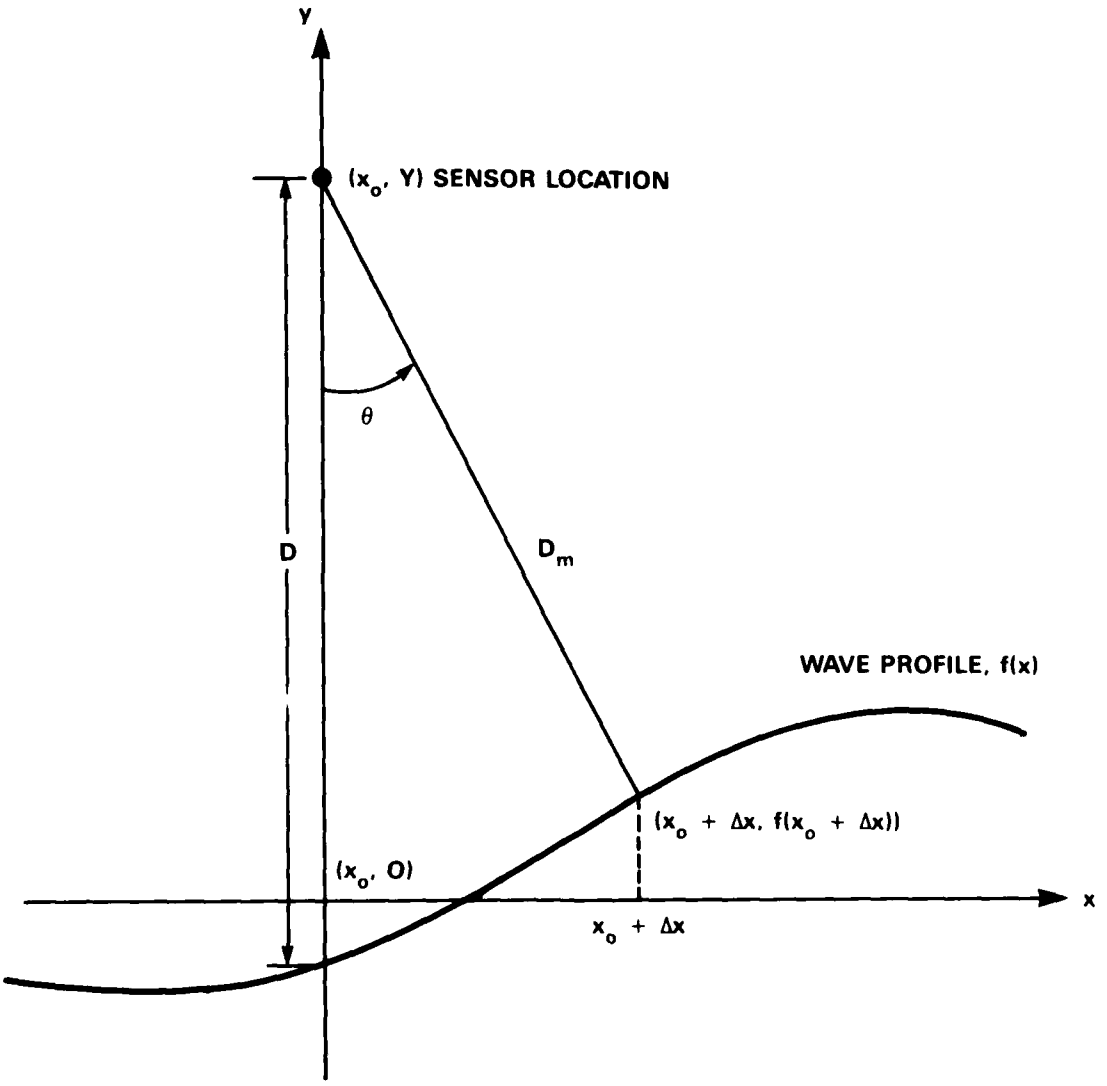

Figure 1 - Sensor and Wave Profile Geometry

$$D_m^2 = \Delta x^2 + (f(x_o+\Delta x)-Y)^2 \tag{1}$$

A maximum or minimum occurs when $\partial D_m^2/\partial \Delta x = 0$, so

$$\frac{\partial D_m^2}{\partial \Delta x} = 2\Delta x + 2\,(f(x_o+\Delta x)-Y)\; f_x(x_o+\Delta x) = 0 \tag{2}$$

where Y is a constant. The maximum or minimum values for D_m occur when Δx is given by

$$\Delta x = f_x(x_o+\Delta x)\;(Y-f(x_o+\Delta x)) \tag{3}$$

The second requirement is to find the outward normals from the profile that will pass through the point (x_o, Y). Figure 2 presents the geometry for this condition. The equation for the line from $(x_o+\Delta x, f(x_o+\Delta x))$ to (x_o, Y) is

$$y = -\frac{1}{f_x(x_o+\Delta x)}\,(x-x_o) + Y \tag{4}$$

At $x = x_o + \Delta x$, $y = f(x_o+\Delta x)$ so

$$f(x_o+\Delta x) = -\frac{1}{f_x(x_o+\Delta x)}\,\Delta x + Y \tag{5}$$

solving for Δx gives

$$\Delta x = f_x(x_o+\Delta x)\;(Y-f(x_o+\Delta x)) \tag{6}$$

The same solution for Δx occurs for either condition. The maximum or minimum distance points on the profile have the characteristic that the outward normal at these points are directed toward the sensor.

Maximum distance points also satisfy these relationships. A criterion is established that will prevent these points from being used in the analytical model. This criterion limits the range of applicability of this model.

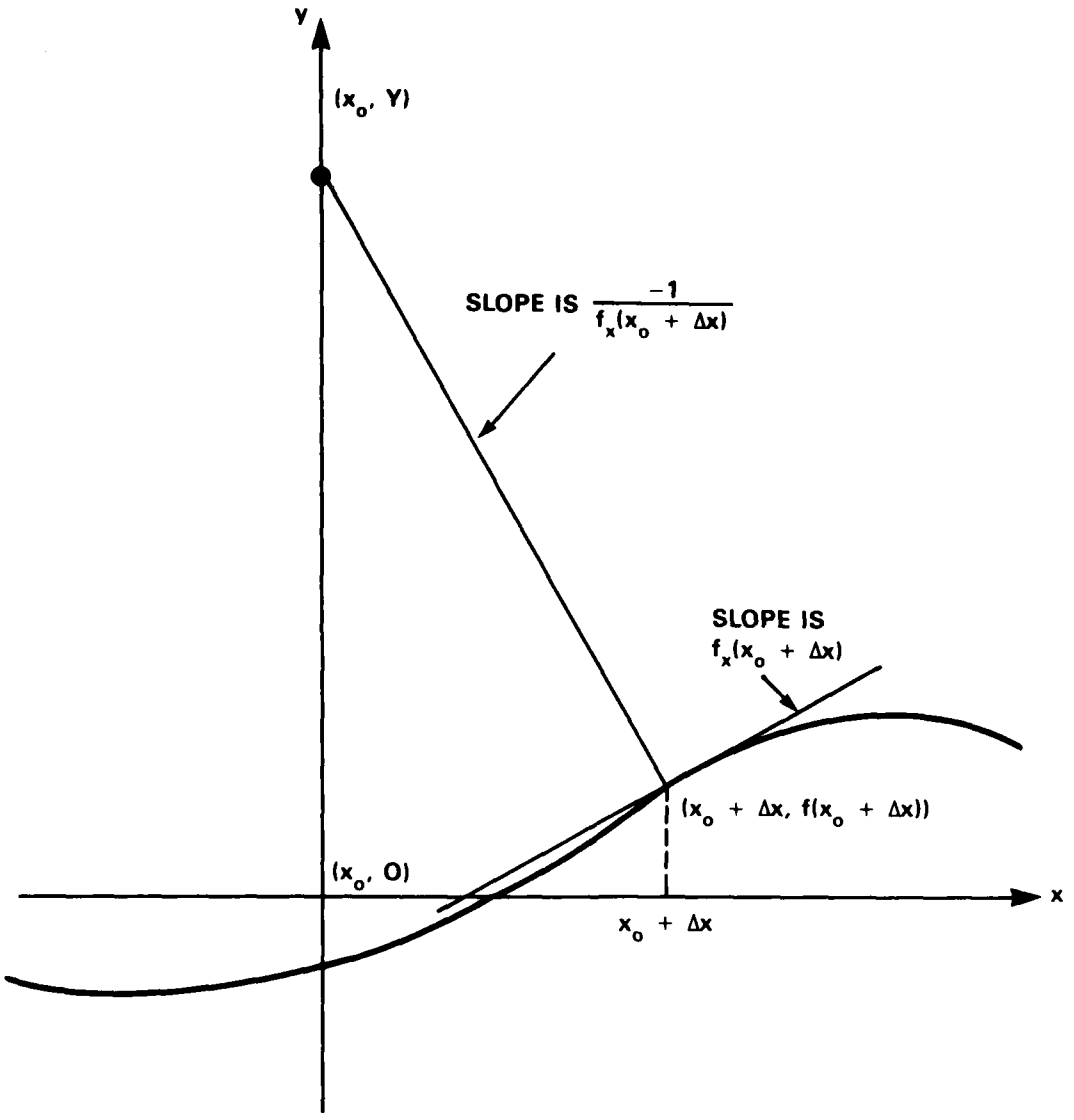

Figure 2 - Sensor and Wave Profile Geometry for Normal Reflections

An example of when a maximum point is detected by the analytical model is given in Figure 3a. The real sensor chooses the closest point, point B in this example; the analytical model, however, chooses point A, a maximum distance point. The analytical model predicts less error in this example.

One approach that prevents the analytical model from selecting maximum distance points is to limit the radius of curvature of the input profile. Figure 3b shows three curves with different curvature. The radius of curve C_2 is the vertical distance from the sensor to the profile. The radius of curve C_1 is less than and the radius of C_3 is more than the radius of C_2. For this example the sonic return comes from every point on curve C_2, but only from point A for curve C_3. For curve C_1, a return comes from point A; however, this profile eventually curves downward and crosses curve C_2. After it changes curvature but before it crosses curve C_2 a minimum occurs. Point B is an example. This minimum is detected by the actual sensor; however, the analytical model chooses point A. The criterion is to bound any radius of curvature in the input profile by the distance from the sensor to the profile. This criterion is described by

$$R_c > Y - f(x) \tag{7}$$

where the radius of curvature, R_c, is

$$R_c = \frac{(1+f_x^2(x))^{3/2}}{| f_{xx}(x) |} \tag{8}$$

so

$$Y - f(x) < \frac{(1+f_x^2(x))^{3/2}}{| f_{xx}(x) |} \tag{9}$$

3.2. MEASURED WAVE HEIGHT

The equations derived for the measured wave height and the return angle are general in that no assumptions are made with respect to the type of input profile seen by the sensor. The measured wave height equation relates the wave height directly beneath the sensor to the wave height measured by the sensor; this is a nonlinear relationship. Since the angle from which the first echo is returned is of

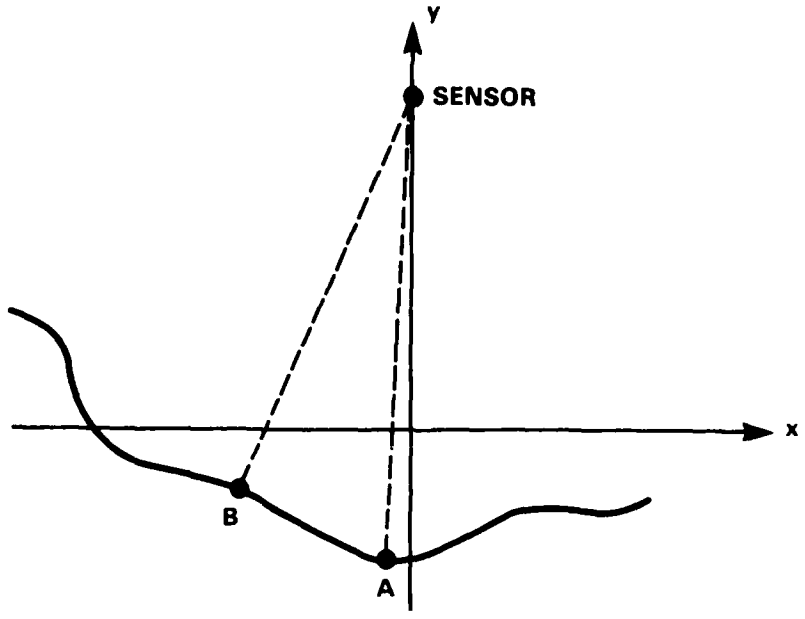

Figure 3a - Detection of a Maximum Point (Point A) by the Analytical Model

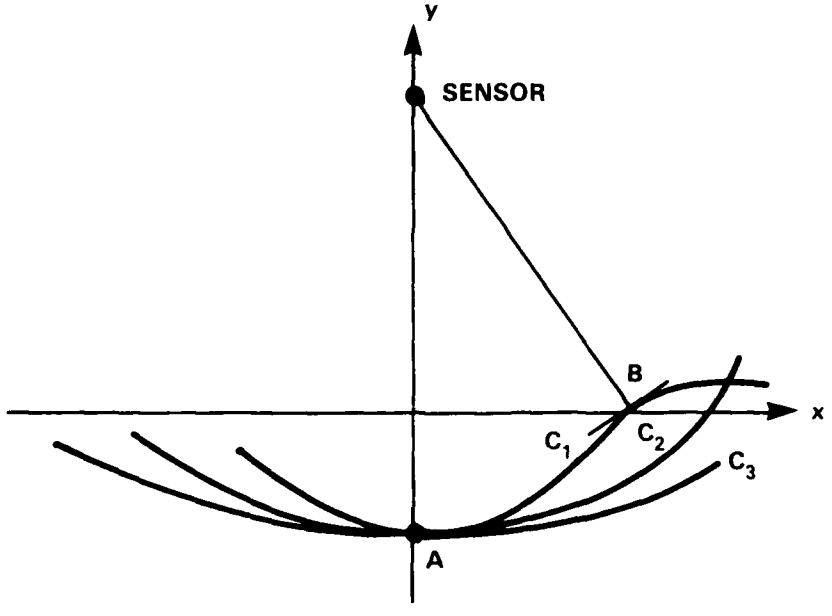

Figure 3b - Radius of Curvature for Three Profiles

Figure 3 - Sensor and Wave Profile Geometry for Two Cases

interest when examining required sensor beamwidths, this equation is also derived.

The geometry used in this derivation is given in Figure 1. Since the profile is assumed to be fixed in time during each sample, partial derivatives denote spatial derivatives of the wave profile. Y is the height of the sensor above the undisturbed water surface, a constant. If the sensor measured the distance to a point directly beneath it, then D would be the actual distance measured. θ is the angle from which the first echo is returned. Although time dependence is not shown in the arguments for these terms, they are all functions of time (except Y). Since the wave profile, f(x), slips beneath the sensor with time, it obeys a wave dispersion relationship.

From Equations (1) and (3), the distance, D_m, measured by the sensor is

$$D_m^2 = \Delta x^2 + (f(x_o+\Delta x)-Y)^2 \tag{10}$$

subject to the constraint

$$\Delta x = f_x(x_o+\Delta x)\ (Y - f(x_o+\Delta x)) \tag{11}$$

so,

$$D_m = (Y - f(x_o+\Delta x))\ (1 + f_x^2(x_o+\Delta x))^{1/2} \tag{12}$$

The measured wave height equation is derived from Equations (11) and (12) using order of magnitude analysis. First, the order of magnitude of each term in these equations is estimated. Linear wave theory (small amplitude) is assumed, so the displacement of the free surface, f, is of order a such that $|f| < a$. The linear displacement, x, is on the order of a wave length, λ. The sensor height above the undisturbed free surface, Y, is also on the order of a wave length. After normalizing these terms, x is order one, Y is order one and the wave height is

$$f = \frac{O(a)}{O(\lambda)} = O(\varepsilon) \tag{13}$$

where ε is a wave slope parameter. All spatial derivatives of f are therefore to order ε. From Equation (11), the order of Δx is obtained. Since

$$\Delta x = f_x(x_o+\Delta x)\ (Y - f(x_o+\Delta x)) \tag{14}$$

then

$$O(\Delta x) = O(\varepsilon)\ (O(1) - O(\varepsilon)) \tag{15}$$

so Δx is of order ε. Each term of Equations (11) and (12) are expanded in a Taylor series to order ε^3; expansions to this order are chosen because expansions to a lower order would not show sensor height dependence in the linear transfer function.

In Equation (12), the expansion of the first term is

$$f(x_o+\Delta x) = f + \Delta x f_x + \frac{\Delta x^2}{2} f_{xx} \tag{16}$$

The argument x_o is dropped since all the terms now have the same argument. For the second term,

$$(1 + f_x^2(x_o+\Delta x))^{1/2} = (1 + f_x^2)^{1/2} + \Delta x \frac{f_x f_{xx}}{(1+f_x^2)^{1/2}} \tag{17}$$

To order ε^3

$$(1 + f_x^2)^{1/2} = 1 + \frac{1}{2} f_x^2 \tag{18}$$

and (also to order ε^3)

$$\Delta x \frac{f_x f_{xx}}{(1+f_x^2)^{1/2}} = \Delta x\ f_x f_{xx} \tag{19}$$

so Equation (17) becomes

$$(1 + f_x^2\ (x_o+\Delta x))^{1/2} = 1 + \frac{1}{2} f_x^2 + \Delta x\ f_x f_{xx} \tag{20}$$

Retaining only the terms to order ε^3, Equation (12) becomes

$$D_m = Y - f + \frac{1}{2} Y f_x^2 - \frac{1}{2} f f_x^2 - \Delta x f_x + Y \Delta x f_x f_{xx} - \frac{D_x^2}{2} f_{xx} \tag{21}$$

The constraint given by Equation (11) is expanded. When Δx is used in Equation (21), it need only be expanded to order ε^2 since it is multiplied by terms of order ε. So the first term in Equation (11) is

$$f_x (x_o + \Delta x) = f_x + \Delta x f_{xx} \tag{22}$$

Using Equation (16) only to order ε^2 and Equation (22), Equation (11) becomes

$$\Delta x = (Y-f) f_x + \Delta x (Y-f) f_{xx} - \Delta x f_x^2 \tag{23}$$

Solving this equation for Δx,

$$\Delta x = \frac{(Y-f) f_x}{1 - (Y-f) f_{xx} + f_x^2} \tag{24}$$

To order ε^2

$$(1 - (Y-f) f_{xx} + f_x^2)^{-1} = 1 + (Y-f) f_{xx} - f_x^2 \tag{25}$$

so, after dropping all terms higher than order ε^2, Equation (24) is

$$\Delta x = (Y-f) f_x + Y^2 f_x f_{xx} \tag{26}$$

To solve for D_m, Equation (26) is applied to Equation (21). Retaining only the terms to order ε^3,

$$D_m = Y - f - \frac{1}{2} Y f_x^2 + \frac{1}{2} f f_x^2 - \frac{1}{2} Y^2 f_x^2 f_{xx} \tag{27}$$

The measured wave height, f_m, is defined as

$$f_m \equiv Y - D_m \tag{28}$$

Using this expression, the measured wave height equation is

$$f_m = f + \frac{1}{2} Y f_x^2 - \frac{1}{2} f f_x^2 + \frac{1}{2} Y^2 f_x^2 f_{xx} \tag{29}$$

to order ε^3.

3.3 LIMIT OF APPLICABILITY FOR ANALYTICAL MODEL

The constraint that allows only minima is approximated using order of magnitude analysis. To order ε, Equation (9) becomes

$$Y < \frac{1}{|f_{xx}|} \tag{30}$$

To order ε, the applicability limit is not precise; however, it will identify the region where the analytical model becomes less valid.

3.4. ECHO RETURN ANGLE

The angle of the returned sonic echo, θ, is given by the geometry as

$$\theta = f_x (x_o + \Delta x) \tag{31}$$

in radians. Since only general estimates of the return angle are required, this equation is expanded to order ε. This angle, in degrees, is

$$\theta = \frac{360}{2\pi} f_x \tag{32}$$

4. APPLICATION OF THE ANALYTICAL MODEL TO SINUSOIDAL WAVE PROFILES

For model testing, regular waves (a sinusoidal profile) are commonly used. The equations are derived that characterize the distortion obtained when using a sonic wave height sensor with this form of wave profile.

Sinusoidal waves have the profile

$$f = A \sin \psi \tag{33}$$

where

$$\Psi = kx - \omega t \tag{34}$$

A is the single amplitude. K is the wave number

$$K = 2\pi/\lambda \tag{35}$$

where λ is the wave length. And, ω is the angular frequency in radians per second.

To find the measured wave profile, Equation (29) is used.

$$f_m = f + \frac{1}{2} Y f_x^2 - \frac{1}{2} f f_x^2 + \frac{1}{2} Y^2 f_x^2 f_{xx} \tag{36}$$

Since

$$f = A \sin \Psi \tag{37}$$

then

$$f_x = A k \cos \Psi \tag{38}$$

and

$$f_{xx} = - A k^2 \sin \Psi \tag{39}$$

so

$$f_m = A \sin \Psi + \frac{1}{2} Y A^2 k^2 \cos^2 \Psi - \frac{1}{2} A^3 k^2 (1+Y^2k^2) \sin \Psi \cos^2 \Psi \tag{40}$$

Since

$$\cos^2 \Psi = \frac{1}{2} (1+\cos 2\Psi) \tag{41}$$

and

$$\sin \Psi \cos^2 \Psi = \frac{1}{4} \sin \Psi + \frac{1}{4} \sin 3\Psi \tag{42}$$

then

$$f_m = \frac{1}{4} Y A^2 k^2 + A \left(1 - \frac{1}{8} A^2 k^2 (1+Y^2 k^2)\right) \sin\Psi$$
$$+ \frac{1}{4} Y A^2 k^2 \cos 2\Psi - \frac{1}{8} A^3 k^2 (1+Y^2 k^2) \sin 3\Psi \tag{43}$$

This equation describes the mean shift, the second harmonic term and the fundamental from which the linear transfer function is obtained. In the next section, the second harmonic amplitude is numerically calculated. The match between the analytical model and these calculations is close for this amplitude, but the model is becoming less accurate. The third harmonic term in Equation (43) will be even less accurate, so only the first three results are examined in detail. The mean shift, μ_{f_m}, is normalized by the sensor height, Y, to form the mean bias

$$\frac{\mu_{f_m}}{Y} = \frac{1}{4} A^2 k^2 \tag{44}$$

The second harmonic amplitude, A_2, is also normalized by the sensor height

$$\frac{A_2}{Y} = \frac{1}{4} A^2 k^2 \tag{45}$$

The linear transfer function, $H(\omega)$, is the fundamental divided by the single amplitude, A, of the wave

$$H(\omega) = 1 - \frac{1}{8} A^2 k^2 (1+Y^2 k^2) \tag{46}$$

Note that the action of the sonic wave height sensor does not distort the phase of the transfer function; phase shift relationships between waves and a test model are not distorted by this error. Since the wave number, k, is 2π divided by the wave length, the terms containing Ak can be rewritten as 2π (A/λ) and the Yk terms as 2 (Y/λ).

The nondimensional A/λ term describes the wave slope and the nondimensional Y/λ term is the sensor height to wave length ratio. The mean bias equation can be rewritten and solved for the wave slope; if experimental measurements of mean shift are obtained, then they can be converted into measurements of wave slope. Measurements or assumptions about the wave length are not necessary.

From the order of magnitude analysis, the mean bias and the second harmonic amplitude are of order ε^2. The second term in the linear transfer function represents the error due to the sonic sensor; this term is also of order ε^2.

The second term in this transfer function equation consists of two parts: a constant term and a term dependent on the sensor height to wave length ratio. This second term is wave length (or frequency) dependent. The sensor height can be adjusted to reduce the second error term; however, regardless of wave length, the first error term produces a bias in the transfer function that is constant with respect to wave length. The error contribution from both terms is equal when $Yk = 1$, so this limit can be used to establish a maximum sensor height.

The angle of the returned sonic burst is given by Equation (31). Applying this equation to the sinusoidal profile gives

$$\theta = \frac{360}{2\pi} A\, k \cos \Psi \tag{47}$$

in degrees. The amplitude or maximum value of the return angle, θ_p, is then

$$\theta_p = 360\, \frac{A}{\lambda} \tag{48}$$

in degrees.

The applicability region for these results is given by Equation (30). For the second derivative given by Equation (39), this region is

$$Y\, A\, k^2 < 1 \tag{49}$$

or

$$\frac{Y}{\lambda}\,\frac{A}{\lambda} < \frac{1}{(2\pi)^2} \tag{50}$$

The peak value of the second derivative is used to establish this bound.

5. NUMERICAL SOLUTION OF THE MEASURED WAVE HEIGHT FOR THE SINUSOIDAL WAVE PROFILE

The measured wave height was calculated for a sinusoidal wave profile and these results are compared to the analytical model. Numerical solutions for the measured wave height were obtained using algorithms implemented on a digital computer. A sinusoidal profile was shifted horizontally under a point representing the ultrasonic displacement sensor. For each position, the minimum distance from this point to the profile was calculated to a given level of accuracy. This distance and the vertical height from the profile to the sensor represent the measured wave height and the actual wave height. These distances and the echo return angle were then stored for each profile shift over a complete wave length. Next, this stored data was processed. The maximum return angle was extracted, and a harmonic analysis was obtained for the measured wave height. This harmonic analysis produced the zero offset and the amplitude and phase of the fundamental frequency component and its harmonics; the mean bias, the second harmonic amplitude and the linear transfer function were obtained from these results. This procedure was then repeated for a variety of wave amplitude to wave length ratios (0.008 to 0.080) and sensor height to wave length ratios (0.1 to 1.0). The results from this numerical calculation are compared to the analytical model. This comparison demonstrates the range of applicability of the analytical model to sinusoidal wave profiles.

5.1. CALCULATION PROCEDURE

Since the sinusoidal profile under the sensor could be at any phase shift relative to the sensor's location, the profile was examined at 128 points throughout a horizontal distance equal to one wavelength. For the region examined, the sensor was located at the middle. The closest point from the sampled profile to the sensor was located and its coordinates stored. Iterative techniques were then used to refine the calculation of the nearest point.

The condition that is satisfied when the nearest point is located is Equation (2); the first derivative is zero. The iterative procedure involves finding the root of this equation. To find this root, a new equation is formed

$$R(\Delta x) = \Delta x + f_x(x_o+\Delta x)\ (f(x_o+\Delta x)-Y) \qquad (51)$$

A value for Δx is tried in this equation and if the remainder $R(\Delta x)$ is nonzero then

a root has not yet been found. The closest point from the sampled profile is used as this initial point. Next, Δx is adjusted and the process is repeated until $R(\Delta x)$ is sufficiently close to zero. The following procedure is used to adjust Δx. If $\Delta x + \xi$ is a root, then expand $R(\Delta x+\xi)$ in a truncated Taylor series

$$R(\Delta x+\xi) = R(\Delta x) + \xi \left.\frac{\partial R(x)}{\partial x}\right|_{x=\Delta x} \tag{52}$$

Since $R(\Delta x+\xi)$ is zero at a root, then

$$\xi = - \frac{R(\Delta x)}{\left.\frac{\partial R(x)}{\partial x}\right|_{x=\Delta x}} \tag{53}$$

The value $\Delta x+\xi$ is then tried in Equation (51). Successive trials are made until the condition

$$\left| \frac{R(\Delta x)}{Y} \right| < 0.00001 \tag{54}$$

is obtained. So $\Delta x/Y$ is found to a tolerance of 0.00001; this implies that the return angle is found to a nominal tolerance of 0.0006 degrees.

The coordinates of this point on the profile are then stored. The profile is shifted and the entire calculation process is repeated until the profile has been shifted one complete wavelength.

5.2. PROCESSING OF STORED MINIMUM POINT COORDINATES

The coordinates of the point on the profile that is the closest point to the sensor were obtained each time the profile was shifted by a distance of $\lambda/128$. For a given wavelength, each shift is equivalent to a change in time for the traveling wave. For the complete wavelength, 128 of these samples were obtained. Using the geometry given in Figure 1, these coordinate values were then used to obtain samples of the measured wave height and the return angle. Samples of the actual wave height were also obtained. These samples were then processed in the following manner.

The maximum return angle was obtained from the return angle samples using standard comparison techniques.

The discrete Fourier transform of the actual wave height and the measured wave height samples produced the mean offset, and the amplitude and phase of the fundamental and its harmonics. A Fast Fourier Transform (FFT) algorithm with an FFT size of 128 performed the Fourier series of these discrete uniformly spaced samples. Taking the Fourier series of the actual wave height provided a check on the operation of the algorithm. The results from the FFT were converted into the amplitude and phase coefficients for a sine series. The first term of this series is the mean offset which is converted into the mean bias by dividing by the sensor height, Y. The second term of this series is the amplitude of the fundamental, so the linear transfer function is the ratio of the measured wave amplitude to the actual wave amplitude. The third term of this series is the amplitude of the second harmonic.

5.3. CALCULATION RESULTS AND COMPARISON TO ANALYTICAL MODEL

Numerical solution for the measured wave height using a sinusoidal profile was obtained using these procedures for 10 wave slope ratios from 0.008 to 0.08 and for 10 sensor height to wavelength ratios from 0.1 to 1.0. These calculations produced results for the return angle, mean bias, the linear transfer function, and the second harmonic amplitude. These calculated results are compared to results using the analytical model. The purpose of this comparison is to demonstrate the range of applicability of the analytical model to sinusoidal profiles.

5.3.1. Maximum Sonic Return Angle

The maximum sonic return angle results are presented in Figure 4. The analytical model results are a single line that was plotted using Equation (48). For the calculated results, all of the maximum return angles converge to the same value for the sensor height to wave length ratio, Y/λ, from 0.1 to 1.0 over the wave slope interval from 0 to 0.04. For the wave slope interval from 0.04 to 0.08, the return angles converge for Y/λ from 0.1 to 0.5. If the region of applicability predicted by Equation (50) was used to delete any calculated return angles for conditions that exceeded this level, then only the results for Y/λ from 0.1 to 0.5 would be plotted. The minor deviation from the analytical model for wave slopes above 0.04 are due to other effects, such as terms higher than order ε.

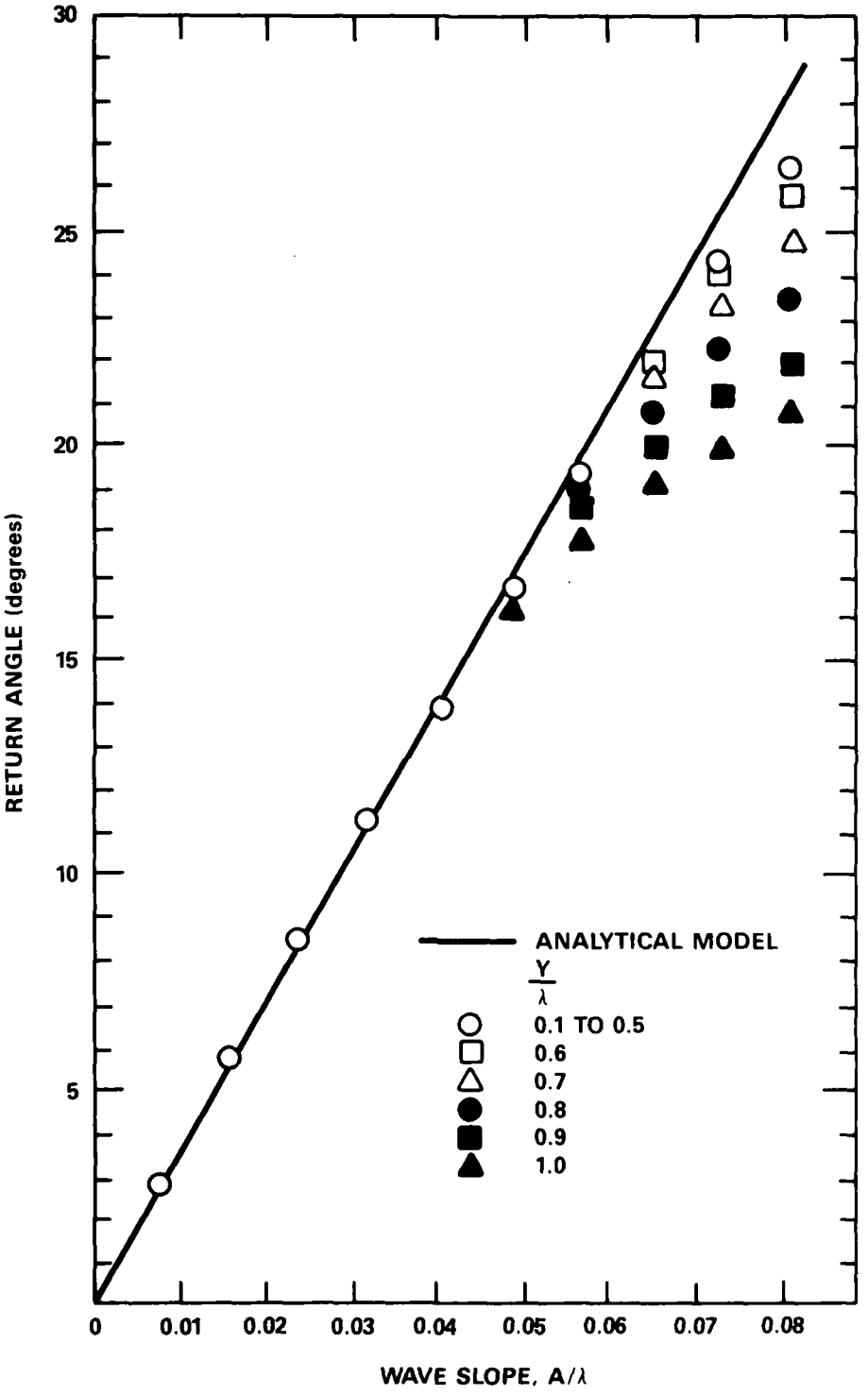

Figure 4 - Return Angle for Sinusoidal Wave Profiles

5.3.2. Mean Bias

The mean bias results are presented in Figure 5. The analytical model results are a single curve that was plotted using Equation (44). For the calculated results, all the mean bias values converge to the same value for Y/λ in the interval from 0.1 to 1.0 over the wave slope interval from 0 to 0.032. For the wave slope interval from 0.032 to 0.08, the mean bias values converge for Y/λ from 0.1 to 0.4. The calculated results are within the region of applicability predicted by Equation (50) provided Y/λ is below 0.3 at $A/\lambda = 0.08$ or Y/λ below 0.4 at $A/\lambda = 0.064$. All of the calculated results that are within the predicted applicability region are very close to the analytical model results. Terms higher than order ε^3 do not significantly affect the quality of the analytical model.

5.3.3. Linear Transfer Function

The linear transfer function results are presented in Figure 6. The analytical model results are a series of curves for wave slope ratios of 0.008, 0.024, 0.04, 0.056, and 0.072; these results were plotted using Equation (46). The transfer function is plotted against the sensor height to wavelength ratio, Y/λ. The calculated results are plotted with each analytical curve; these results are either on or slightly above each curve. The phase angle of the transfer function is zero for both the analtytical model and the calculated results. The region of applicability for the analytical model given by Equation (50) produced the applicability limit denoted by the dashed line on Figure 6; any analytical model result below this line does not satisfy this inequality. In the region above this line, the calculated and analytical model results match very closely; differences are attributed to terms higher than order ε^3.

5.3.4. Second Harmonic Amplitude

The second harmonic amplitude results are presented in Figure 7. The second harmonic amplitude, A_2, is normalized by the sensor height, Y. The analytical model results are a single curve that was plotted using Equation (45). For the calculated results, the results for Y/λ of 0.1 are presented. Using the applicability limits given by Equation (50), the largest Y/λ result that is still within this limit for a given wave slope ratio is also plotted; the Y/λ value is printed next to each point. For wave slopes up to about 0.024, the match between the calculated and the analytical model is good; beyond this region, significant differences exist. Only results

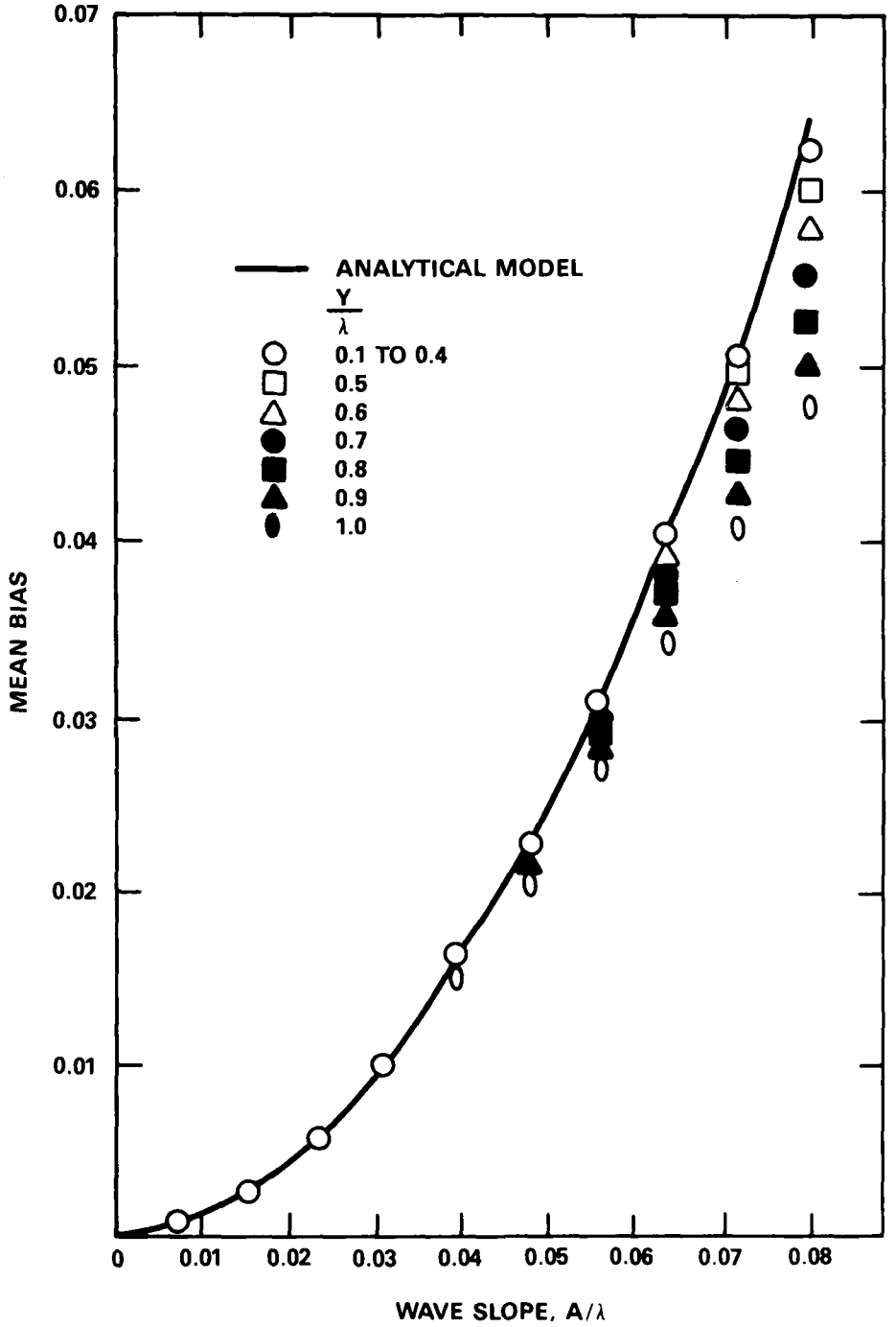

Figure 5 - Mean Bias for Sinusoidal Wave Profiles

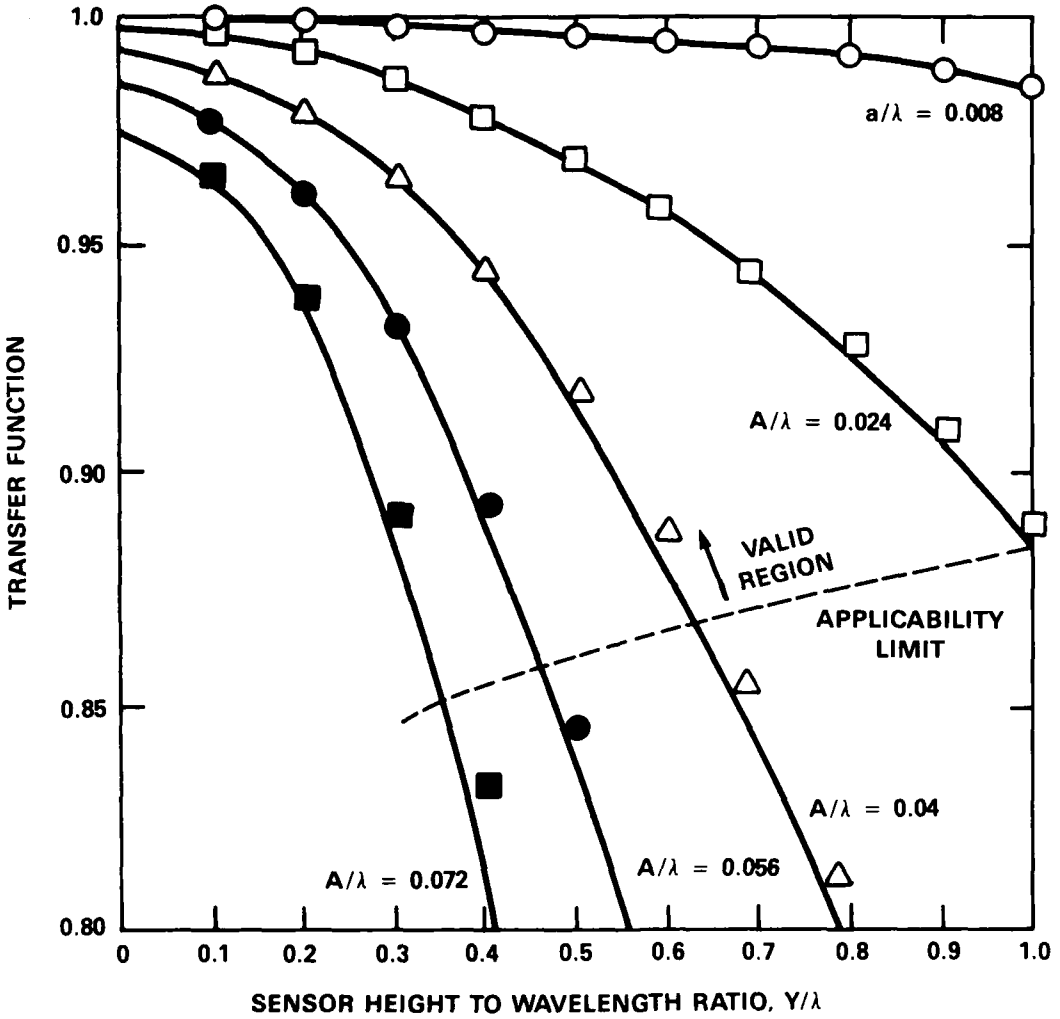

Figure 6 - Linear Transfer Function for Sinusoidal Wave Profiles

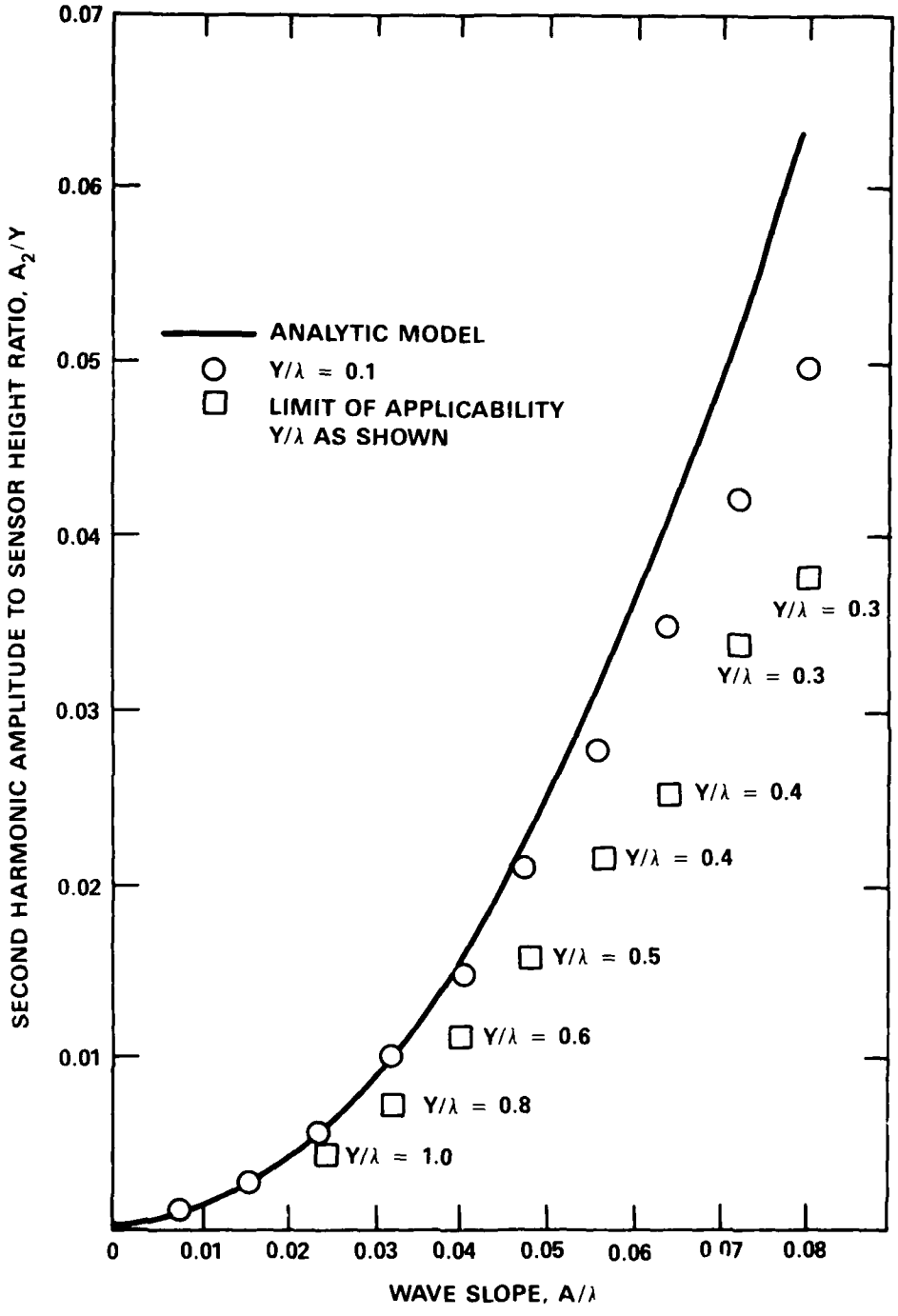

Figure 7 - Second Harmonic Amplitude to Sensor Height Ratio for Sinusoidal Wave Profiles

within the applicability limit are presented, so the discrepancy in the analytical model is due to terms higher than order ϵ^3. Expansions to higher order terms are necessary before the analytical model will match the calculated values over an extended region. The analytical model does over estimate the amount of second harmonic distortion, so in its present form, it still has value when estimates of the second harmonic distortion are required.

6. APPLICATION OF THE ANALYTICAL MODEL TO RANDOM WAVE PROFILES

Random waves are used in model testing to simulate ocean wave conditions. Statistical methods are employed to characterize a random seaway. These random processes are assumed to be zero mean and Gaussian distributed.

6.1. MEAN VALUE OF MEASURED WAVE HEIGHT

For Random processes, the expectation operator, $E[\cdot]$, gives the mean or expected value. Applying this operator to Equation (29), the mean value of the measured wave height is μ_{f_m}.

$$\mu_{f_m} = E[f_m] = E[f + \frac{1}{2} Y f_x^2 - \frac{1}{2} f f_x^2 + \frac{1}{2} Y^2 f_x^2 f_{xx}] \tag{55}$$

Since the expectation operator is linear, and using the properties of Gaussian random processes summarized in Appendix A, then

$$\mu_{f_m} = \frac{1}{2} Y E[f_x^2] \tag{56}$$

Since f_x is zero mean,

$$\mu_{f_m} = \frac{1}{2} Y \sigma_{f_x}^2 \tag{57}$$

The mean bias is then

$$\frac{\mu_{f_m}}{Y} = \frac{1}{2} \sigma_{f_x}^2 \tag{58}$$

As is shown next, the mean bias is of order ε^2.

The variance of the wave slope, $\sigma^2_{f_x}$, is now evaluated. This variance is related to the auto spectrum of the wave slope, $S_{f_x f_x}(\omega)$, by

$$\sigma^2_{f_m} = \int_0^\infty S_{f_x f_x}(\omega)\, d\omega \tag{59}$$

The wave slope variance is of order ε^2, so the mean bias is also of order ε^2. The transfer function of the spatial derivative is ik where k is the wave number, so the auto spectrum of f, $S_{ff}(\omega)$, is related to $S_{f_x f_x}(\omega)$ by

$$S_{f_x f_x}(\omega) = k^2\, S_{ff}(\omega) \tag{60}$$

Therefore

$$\sigma^2_{f_x} = \int_0^\infty k^2\, S_{ff}(\omega)\, d\omega \tag{61}$$

The wave number's dependence on frequency is given by the dispersion relationship. Deep water waves are assumed, so this relationship is

$$\omega^2 = gk \tag{62}$$

where g is the gravitational constant. The relationship for the wave slope variance is then

$$\sigma^2_{f_x} = \frac{1}{g^2} \int_0^\infty \omega^4\, S_{ff}(\omega)\, d\omega \tag{63}$$

During basin experiments, the mean value of the sonic sensor's output signal can be measured. After rewriting the mean bias equation (Equation (58)) in terms of the wave slope variance, the measured mean value can then provide a measurement of the wave slope variance. A wave dispersion relationship is not assumed for this measurement method.

6.2. LINEAR TRANSFER FUNCTION BETWEEN ACTUAL AND MEASURED WAVE HEIGHT

The transfer function between the actual and measured wave height is derived from their cross spectrum. Since the cross spectrum is the Fourier transform of the cross correlation, the cross correlation function, $R_{ff_m}(\tau)$, is obtained first.

$$R_{ff_m}(\tau) = E[f(t)f_m(t+\tau)] - E[f(t)]\,E[f_m(t+\tau)] \tag{64}$$

The cross correlation function is of order ε^2. From Equation (29), and since f has zero mean, then

$$\begin{aligned} R_{ff_m}(\tau) = E[&f(t)\,f(t+\tau) + \tfrac{1}{2}\,Y\,f(t)\,f_x^2(t+\tau) \\ &- \tfrac{1}{2}\,f(t)\,f(t+\tau)\,f_x^2(t+\tau) \\ &+ \tfrac{1}{2}\,Y^2\,f(t)\,f_x^2(t+\tau)\,f_{xx}(t+\tau)] \end{aligned} \tag{65}$$

Terms to order ε^4 are retained because the correlation function is to order ε^2.

Using the properties of Gaussian random processes described in Appendix A.

$$R_{ff_m}(\tau) = R_{ff}(\tau) - \tfrac{1}{2}\,\sigma_{f_m}^2\,R_{ff}(\tau) + \tfrac{1}{2}\,Y^2\,\sigma_{f_x}^2\,R_{ff_{xx}}(\tau) \tag{66}$$

where

$$\sigma_{f_x}^2 = R_{f_x f_x}(0) \tag{67}$$

The cross spectrum is the Fourier transform of the cross correlation function, so the cross spectrum between the actual and measured wave height, $S_{ff_m}(\omega)$, is

$$S_{ff_m}(\omega) = S_{ff}(\omega) - \tfrac{1}{2}\,\sigma_{f_x}^2\,S_{ff}(\omega) + \tfrac{1}{2}\,Y^2\,\sigma_{f_x}^2\,S_{ff_{xx}}(\omega) \tag{68}$$

The term $S_{ff_{xx}}(\omega)$ is now evaluated by noting that this is the cross spectrum between the wave and its second spatial derivative. Since this transfer function is $(ik)^2$,

$$S_{ff_{xx}}(\omega) = - k^2 S_{ff}(\omega) \tag{69}$$

so

$$S_{ff_m}(\omega) = S_{ff}(\omega) \left(1 - \frac{1}{2}\sigma_{f_x}^2 (1 + (Yk)^2)\right) \tag{70}$$

The transfer function, $H(\omega)$, between the actual and measured wave height is

$$H(\omega) = \frac{S_{ff_m}(\omega)}{S_{ff}(\omega)} = 1 - \frac{1}{2}\sigma_{f_x}^2 (1+(Yk)^2) \tag{71}$$

In general, a transfer function is a complex number; in this case the function is real valued, so no phase distortion exists. The second term of the transfer function represents the error due to the sonic sensor. *This term includes the slope variance,* so this term is of order ε^2.

The second term in this transfer function equation consists of two parts: a constant term and a term dependent on the sensor height to wavelength ratio. This second term is wavelength (or frequency) dependent. The sensor height can be adjusted to reduce the second error term; however, regardless of wavelength, the first error term produces a bias in the transfer function that is constant with respect to wavelength.

6.3. AUTO SPECTRUM AND STANDARD DEVIATION OF THE MEASURED WAVE HEIGHT

The derivation of the auto spectrum and standard deviation of the measured wave height are both obtained from the auto correlation of the measured wave height, $R_{f_m f_m}(\tau)$.

$$R_{f_m f_m}(\tau) = E[f_m(t) f_m(t+\tau)] - E^2[f_m(t)] \tag{72}$$

The mean value in the second term is given by Equation (57); the first term, however, must be expanded using Equation (29). This auto correlation function is of order ε^2. After the expansion of the first term, only the even mixed moments up to order ε^4 are retained.

$$E[f_m(t)\ f_m(t+\tau)] = E[f(t)\ f(t+\tau)]$$

$$- \frac{1}{2} E[f(t)\ f_x^2(t)\ f(t+\tau)] + \frac{1}{2} Y^2 E[f_x^2(t)\ f_{xx}(t)\ f(t+\tau)]$$

$$+ \frac{1}{4} Y^2 E[f_x^2(t)\ f_x^2(t+\tau)] - \frac{1}{2} E[f(t)\ f(t+\tau)\ f_x^2(t+\tau)]$$

$$+ \frac{1}{2} Y^2 E[f(t)\ f_x^2(t+\tau)\ f_{xx}(t+\tau)] \qquad (73)$$

Using the other properties of Gaussian random processes summarized in Appendix A,

$$E[f_m(t)\ f_m(t+\tau)] = R_{ff}(\tau) - \sigma_{f_x}^2 R_{ff}(\tau)$$

$$+ \frac{1}{2} Y^2 \sigma_{f_x}^2 (R_{f_{xx}f}(\tau) + R_{ff_{xx}}(\tau))$$

$$+ \frac{1}{4} Y^2 [\sigma_{f_x}^4 + 2 R_{f_x f_x}^2(\tau)] \qquad (74)$$

Combining Equations (74) and (57) into Equation (72) yields

$$R_{f_m f_m}(\tau) = R_{ff}(\tau) - \sigma_{f_x}^2 R_{ff}(\tau)$$

$$+ \frac{1}{2} Y^2 \sigma_{f_x}^2 (R_{f_{xx}f}(\tau) + R_{ff_{xx}}(\tau))$$

$$+ \frac{1}{2} Y^2 R_{f_x f_x}^2(\tau) \qquad (75)$$

At this point, the variance of the measured wave height, $\sigma_{f_m}^2$, is given by

$$\sigma_{f_m}^2 = R_{f_m f_m}(0) = \sigma_f^2 - \sigma_{f_x}^2 \sigma_f^2$$

$$+ \frac{1}{2} Y^2 \sigma_{f_x}^2 (R_{f_{xx} f}(0) + R_{f f_{xx}}(0))$$

$$+ \frac{1}{2} Y^2 \sigma_{f_x}^4 \tag{76}$$

The terms

$$R_{f_{xx} f}(0) = R_{f f_{xx}}(0) = \int_0^\infty S_{f_{xx} f}(\omega)\, dw \tag{77}$$

From Equation (69)

$$S_{f f_{xx}}(\omega) = S_{f_{xx} f}(\omega) = - k^2 S_{ff}(\omega) \tag{78}$$

so

$$R_{f_{xx} f}(0) = R_{f f_{xx}}(0) = - \int_0^\infty k^2 s_{ff}(\omega)\, dw \tag{79}$$

From Equation (61),

$$R_{f f_{xx}}(0) = - \sigma_{f_x}^2 \tag{80}$$

So the variance of the measured wave height is

$$\sigma_{f_m}^2 = \sigma_f^2 - \sigma_{f_x}^2 \sigma_f^2 - \frac{1}{2} Y^2 \sigma_{f_x}^4 \tag{81}$$

The standard deviation ratio is then

$$\frac{\sigma_{f_m}}{\sigma_f} = \sqrt{1 - \sigma_{f_x}^2 - \frac{1}{2} Y^2 \frac{\sigma_{f_x}^4}{\sigma_f^2}} \tag{82}$$

The auto spectrum of the measured wave height is the Fourier transform of Equation (75). The last term in this equation is a quadratic nonlinearity, it is approximated by zero.

This neglected term is of order ε^4, while the auto spectrum is of order ε^2. To retain consistency in the order of magnitude of the retained terms, this term should not be eliminated. The Fourier transform of this term, however, is tractable only when the wave slope spectrum has a given form.

The Fourier transform of this quadratic nonlinear term, $R^2_{f_x f_x}(\tau)$, will result in the slope spectrum convolved with itself. In the measured wave height spectrum, these components will be distributed at sum and difference frequencies; this action has the effect of placing background noise in frequency regions where the actual wave height spectrum itself would have low spectrum values. Since this term is assumed to be zero, the analytical model results will not account for this effect.

With this term approximated by zero, the autospectrum is then

$$S_{f_m f_m}(\omega) = S_{ff}(\omega) - \sigma_{f_x}^2 S_{ff}(\omega) + \frac{1}{2} Y^2 \sigma_{f_x}^2 (S^*_{ff_{xx}}(\omega) + S_{ff_{xx}}(\omega)) \tag{83}$$

From Equation (69),

$$S_{ff_{xx}}(\omega) = S^*_{ff_{xx}}(\omega) = - k^2 S_{ff}(\omega) \tag{84}$$

And, from Equation (60)

$$S_{f_x f_x}(\omega) = k^2 S_{ff}(\omega) \tag{85}$$

So the auto spectrum of the measured wave height is

$$S_{f_m f_m}(\omega) = S_{ff}(\omega)\ [1 - \sigma_{f_x}^2\ (1+(Yk)^2)] \tag{86}$$

The response amplitude operator or RAO is the ratio

$$\frac{S_{f_m f_m}(\omega)}{S_{ff}(\omega)} = 1 - \sigma_{f_x}^2\ (1+(Yk)^2) \tag{87}$$

6.4. COHERENCY BETWEEN ACTUAL AND MEASURED WAVE HEIGHT

The coherency is defined as

$$\gamma^2(\omega) = \frac{\left| S_{ff_m}(\omega) \right|^2}{S_{f_m f_m}(\omega)\ S_{ff}(\omega)} \tag{88}$$

so from Equations (70) and (86), the coherency between the actual and measured wave height is

$$\gamma^2(\omega) = \frac{[1 - \frac{1}{2}\sigma_{f_x}^2\ (1+(Yk)^2)]^2}{1 - \sigma_{f_x}^2\ (1+(Yk)^2)} \tag{89}$$

To order ε^3, the numerator is

$$[1 - \tfrac{1}{2}\sigma_{f_x}^2\ (1+(Yk)^2)]^2 = 1 - \sigma_{f_x}^2\ (1+(Yk)^2) \tag{90}$$

so

$$\gamma^2(\omega) = 1 \tag{91}$$

6.5. ANGLE OF THE RETURNED SONIC ECHOS

The angle of the returned sonic echo is given by Equation (31) to order ε.

$$\theta = \frac{360}{2\pi} f_x \tag{92}$$

in degrees. Since f_x is zero mean and Gaussian, then θ is also zero mean and Gaussian. The variance of θ is then, in degrees squared,

$$\sigma_\theta^2 = \left(\frac{360}{2\pi}\right)^2 \sigma_{f_x}^2 \tag{93}$$

To order ε, the standard deviation of the echo return angle is

$$\sigma_\theta = \frac{360}{2\pi} \sigma_{f_x} \tag{94}$$

in degrees.

6.6. REGION OF APPLICABILITY FOR THE ANALYTICAL MODEL

The region of applicability of these results is given by Equation (30). The second derivative of the profile, f_{xx}, is Gaussian with zero mean, so the variance of f_{xx} is $\sigma_{f_{xx}}^2$ and f_{xx} will exceed the bounds of $\pm 2\ \sigma_{f_{xx}}$ about five percent of the time. When this bound is used for the applicability limit, Equation (30) becomes

$$Y\ \sigma_{f_{xx}} < \frac{1}{2} \tag{95}$$

The variance, $\sigma_{f_{xx}}^2$, is now evaluated. The auto spectrum of f_{xx} is $S_{f_{xx}f_{xx}}(\omega)$, so the variance is

$$\sigma_{f_{xx}}^2 = \int_0^\infty S_{f_{xx}f_{xx}}(\omega)\ dw \tag{96}$$

The transfer function between f and f_{xx} is $(ik)^2$, so the auto spectrum of f is related to $S_{f_{xx}f_{xx}}(\omega)$ by

$$S_{f_{xx}f_{xx}}(\omega) = k^4 S_{ff}(\omega) \tag{97}$$

So

$$\sigma^2_{f_{xx}} = \int_0^\infty k^4 S_{ff}(\omega)\, dw \tag{98}$$

For the deep water dispersion relationship, Equation (62), this variance is

$$\sigma^2_{f_{xx}} = \frac{1}{g^4} \int_0^\infty \omega^8 S_{ff}(\omega)\, dw \tag{99}$$

7. SIMULATION OF RANDOM WAVE PROFILE

The operation of an ultrasonic displacement sensor was simulated over a random wave profile, the results from this simulation are compared to the analytical model. This comparison demonstrates the range of applicability of the analytical model to random wave profiles.

7.1. SIMULATION PROCEDURE

The simulation used algorithms implemented on a digital computer. The wave profile was stepped in time using the deep water wave dispersion relationship, and the closest point to the location of the ultrasonic displacement sensor for each time step was used to generate what the sensor would measure. For each time step the wave profile was simulated over a horizontal range from +20 to -20 feet in 0.5 foot increments using the sum of 50 irregularly spaced (in frequency) sine waves. In time, 1000 of these profiles were generated in 0.5 second increments. The sensor was located above the center of this profile.

The irregularly spaced sine waves used to produce this profile were selected to approximate the single parameter Pierson-Moskowitz (PM) wave spectrum. Three different sea states were constructed: 1.25, 2.5, and 5 foot significant wave height. (Significant wave height is four times the standard deviation of the wave height.) For each of these sea states, the sensor's time history response was determined for three sensor heights above the undisturbed water level: 6, 11, and 20 feet. Only one profile series was created for each sea state; the same profile series was used for each of these sensor heights.

This simulated random wave profile consists of the sum of 50 sine waves. This profile is random in the sense that each realization or sample function of an ensemble will have random phase for each sine wave component when one component is compared to another. This random process is stationary and ergodic. It is also approximately Gaussian since the probability density function (pdf) of the sum of 50 sine waves is the multiple convolution of each other. From the central limit theorem (see Bendat[2]), the result of this multiple convolution will approach a Gaussian probability density function. Additional details of this simulation are given in Appendix B.

7.2. DATA REDUCTION OF SIMULATED DATA

The actual wave height, measured wave height and return angle time histories obtained from these nine simulation runs were processed using standard statistical analysis algorithms. For the echo return angle, mean and standard deviation estimates were obtained. For the actual and measured wave height, estimates were obtained for mean values, standard deviation, auto spectra, cross spectra, coherency, and the transfer function.

The mean value and standard deviation were estimated using the following equations. The mean value estimate is

$$\hat{\mu}_x = \frac{1}{M} \sum_{m=1}^{M} x_m \tag{100}$$

where x_m are the data samples and M is the total number of samples (sample rate times run length). The standard deviation estimate is

$$\hat{\sigma}_x = \sqrt{\frac{1}{M} \sum_{m=1}^{M} x_m - (\hat{\mu}_x)^2} \tag{101}$$

The auto spectra and cross spectra were estimated using the method of overlapped Fast Fourier Transform (FFT) processing of windowed data segments (see Nuttall[3] and Welch[4]). A 50 percent segment overlap and a full cosine data window are the reduction parameters used for this data reduction. Once these spectral estimates were obtained, the transfer function and coherency were obtained in the following manner. The transfer function estimate is

$$\hat{H}(\omega) = \frac{\hat{S}_{xy}(\omega)}{\hat{S}_{xx}(\omega)} \tag{102}$$

The coherency estimate is

$$\hat{\gamma}^2(\omega) = \frac{\left| \hat{S}_{xy}(\omega) \right|^2}{\hat{S}_{xx}(\omega)\, \hat{S}_{yy}(\omega)} \tag{103}$$

where the random process, x, is the input and y is the output.

7.3. SIMULATION RESULTS AND COMPARISON TO ANALYTICAL MODEL

The purpose of this comparison is to demonstrate the range of applicability of the analytical model to random profiles. The reduction of the simulated data produced estimates of the echo return angle standard deviation, and the measured wave height's mean value, standard deviation and auto spectrum, as well as the cross spectrum, coherency and transfer function between the actual and the measured wave height. These estimates are compared to results using the analytical model.

7.3.1. Wave Slope Variance and Applicability Limit for the Analytical Model

When the analytical model is applied to a random profile, the results are parameterized by the variance of the wave profile's slope or first spatial derivative. Also, the region of applicability of the analytical model is determined by the variance of the profile's second spatial derivative. The equations that relate these terms to the auto spectrum of deep water waves are Equations (63) and (99). For the simulation, this auto spectrum is the PM wave spectrum that was band-limited at 3.613 radians per second. The procedures for deriving these variances analytically from the PM spectrum and from the simulated spectrum are presented in Appendix C.

From either method, both of these variances were calculated for the three significant wave heights: 1.25, 2.5, and 5 feet. These results are presented in Table 1; both methods produce nearly identical results.

For random wave profiles, the region of applicability for these results is given by Equation (95). Rewriting this equation in terms of Y, then

$$Y < \frac{1}{2\sigma_{f_{xx}}} \tag{104}$$

Using the calculated values for $\sigma^2_{f_{xx}}$, the upper limits for Y are given in the last column of Table 1. Since Y = 20 feet was the most extreme sensor height used in the simulation, all of the simulation results are within the range of applicability. Except as noted, any differences between the analytical model and the simulation results are attributed to terms of higher order than ε^3.

TABLE 1 - WAVE SLOPE VARIANCE AND VARIANCE OF SECOND SPATIAL DERIVATIVE FOR SIMULATED RANDOM WAVE DATA

Significant Wave Height (ft)	Wave Slope Variance From (nondimensional)		Variance of Second Spatial Derivative (ft^{-1})		Applicability Limit for Y (ft)
	Equation C.5	Numerical Integration	Equation C.9	Numerical Integration	
1.25	0.00324	0.00335	0.000227	0.000235	33.2
2.5	0.00599	0.00583	0.000292	0.000303	29.3
5.0	0.00871	0.00859	0.000319	0.000330	28.0

7.3.2. Echo Return Angle Mean and Standard Deviation

The return angle standard deviation results are presented in Figure 8. The analytical model results are a single line that was plotted using Equation (94). All of the results from the simulation are very close to the analytical model results. The return angle is independent of sensor height. From the analytical model, the return angle has zero mean; the largest deviation from zero mean in the simulation results was one case where the mean value was 0.07 degrees.

7.3.3. Mean Bias

The mean bias results are presented in Figure 9. The analytical model results are a single curve that is plotted using Equation (58). Except for the cases when the sensor height was 6 feet, the simulation and analytical model results are almost identical. The discrepancy is attributed to terms higher than order ε^3.

7.3.4. Standard Deviation Ratio

The standard deviation ratio results are presented in Figure 10. The analytical

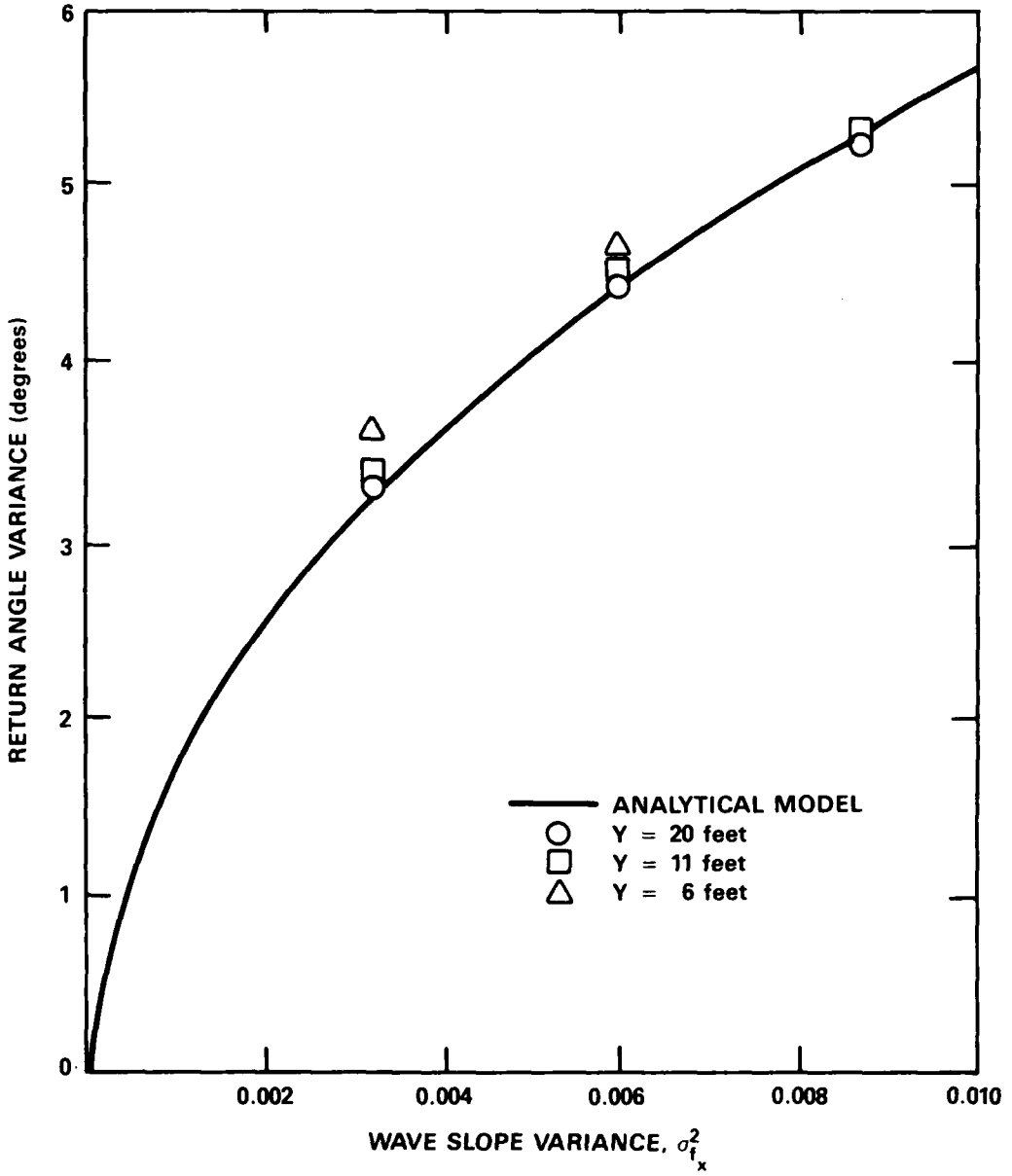

Figure 8 - Return Angle Variance for Random Wave Profiles

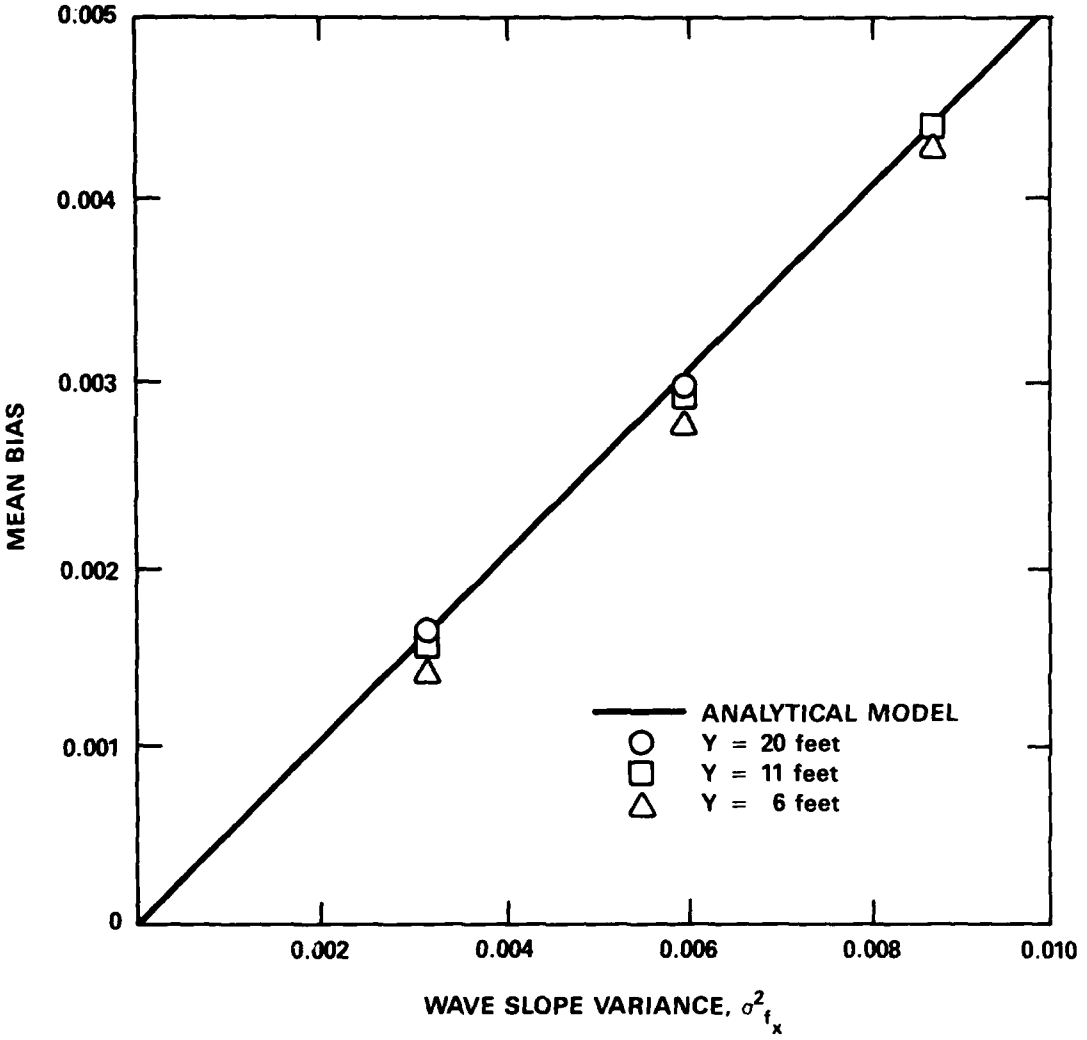

Figure 9 - Mean Bias for Random Wave Profiles

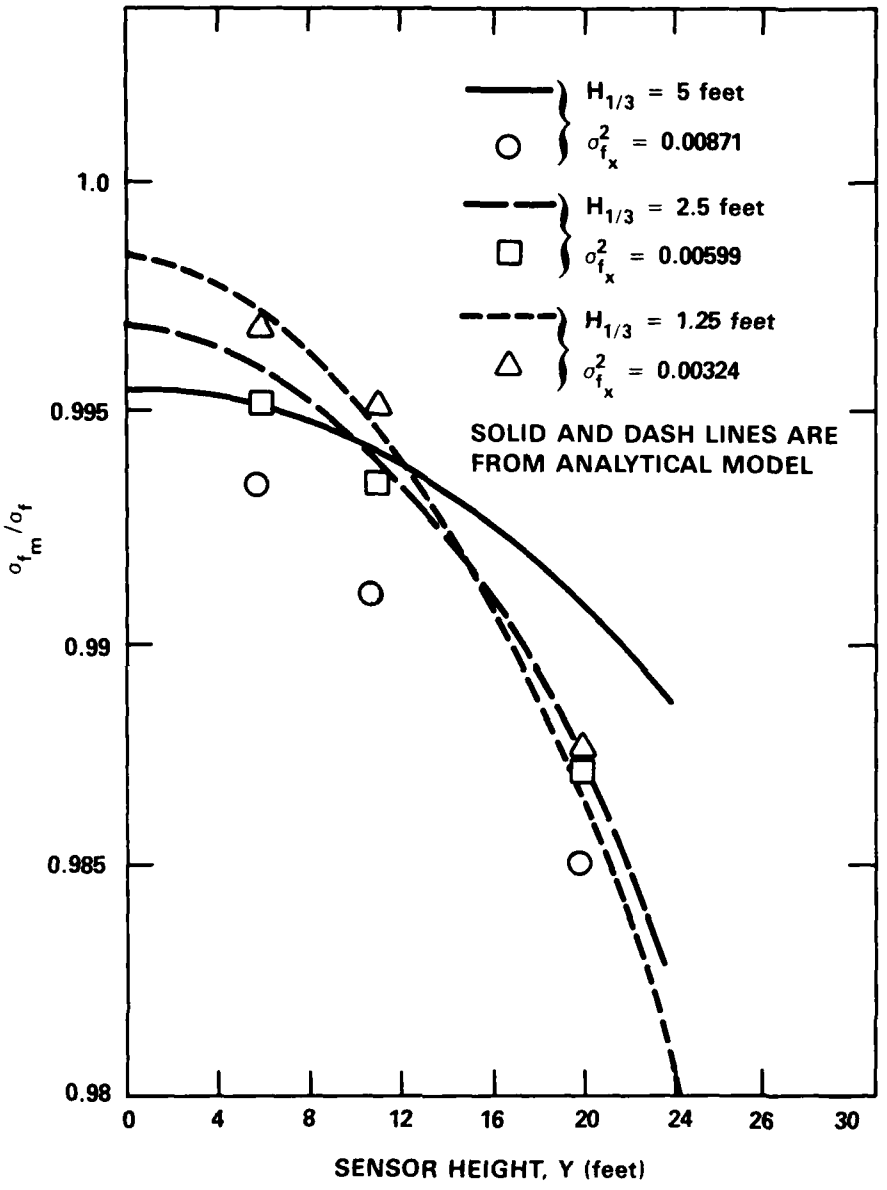

Figure 10 - Standard Deviation Ratio for Measured and Actual Wave Height for Random Wave Profiles

model results are a series of curves for different wave slopes and significant wave heights. These results are plotted from Equation (82). Except for the 5-foot significant wave height cases, the analytical model results closely match the simulation results. Again, terms higher than order ε^3 would produce these differences.

7.3.5. Linear Transfer Function

The linear transfer function results are presented in Figure 11. The analytical model results are three curves for each of the three wave slope variances; these results were plotted using Equation (71). The simulation results came from the three runs made at a sensor height of 20 feet. Although a fair amount of scatter (random error due to finite sample length) exists in the simulation results, these results generally are higher than the analytical model results. This slight reduction is likely due to terms higher than order ε^3. The lower simulation results at low Y/λ values (low frequency) are probably biased by the rapidly increasing input wave spectrum.

From the analytical model, the phase of the transfer function is 0 degrees. The simulation results gave a transfer function phase that scattered very closely about 0 degrees. Figure 12 presents this transfer function phase for one condition.

7.3.6. Auto Spectrum and Response Amplitude Operator

Analytical model and simulation results are presented for one condition: significant wave height of five feet and sensor height of 11 feet. The actual wave height auto spectrum as a function of the sensor height to wavelength ratio is presented in Figure 13. The response amplitude operator (RAO) of the measured wave spectrum to the actual wave spectrum is given in Figure 14. The RAO predicted by the analytical model is plotted on this figure as a continuous curve; Equation (87) was used for this curve. Beyond a Y/λ ratio of 0.35, the analytical model underestimates this RAO; the quadratic nonlinear term neglected in the analytical model derivation is a likely source since the nonlinear action would increase the spectral level at higher frequencies. As seen in the actual wave height spectrum, Figure 13, the spectral values are low beyond Y/λ of 0.35; only a small amount of background noise is required to produce the three to five percent increase seen in the RAO.

7.3.7. Coherency

The coherency results for the condition of 5-foot significant wave height and

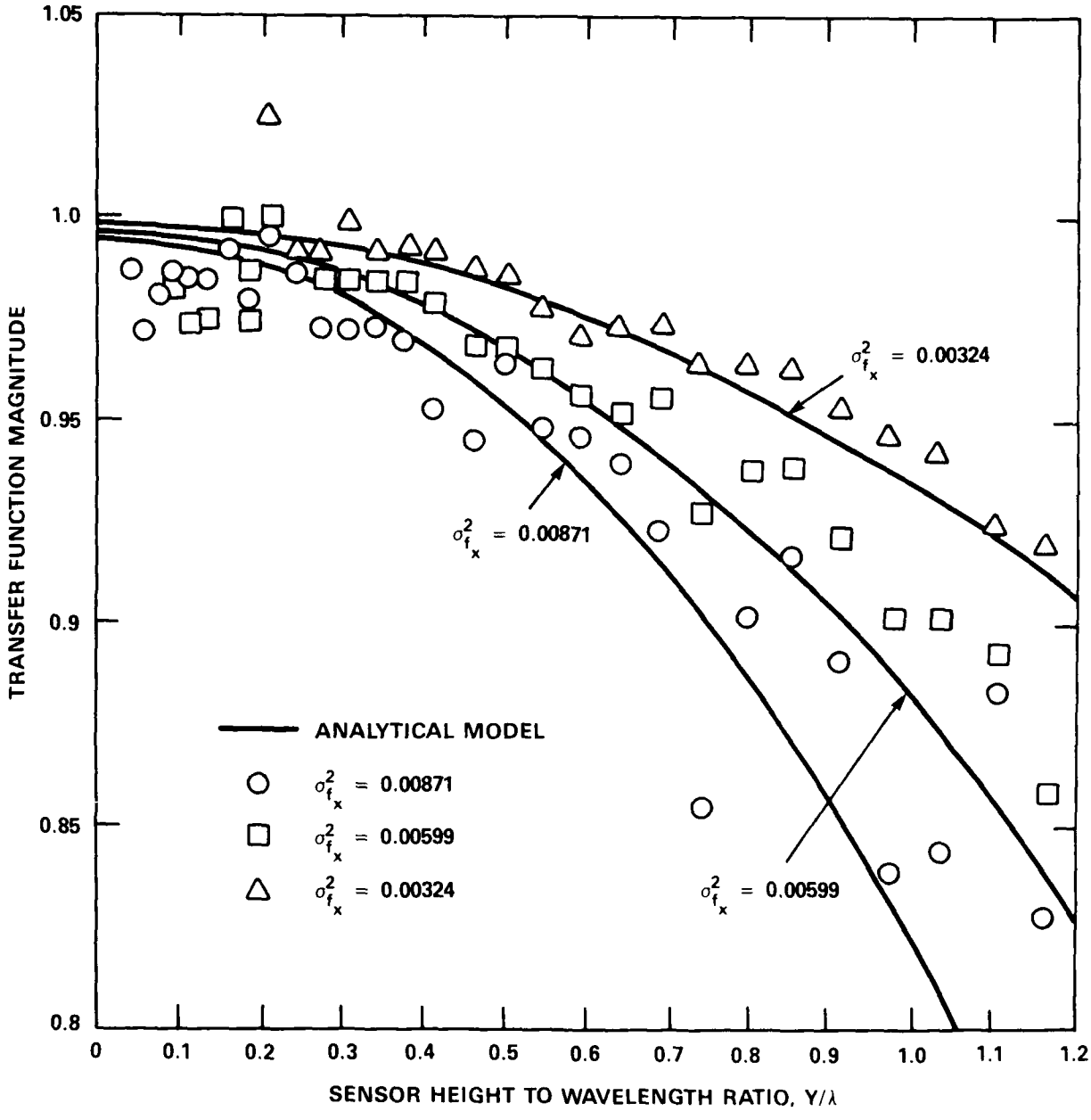

Figure 11 - Transfer Function Magnitude for Random Wave Profiles

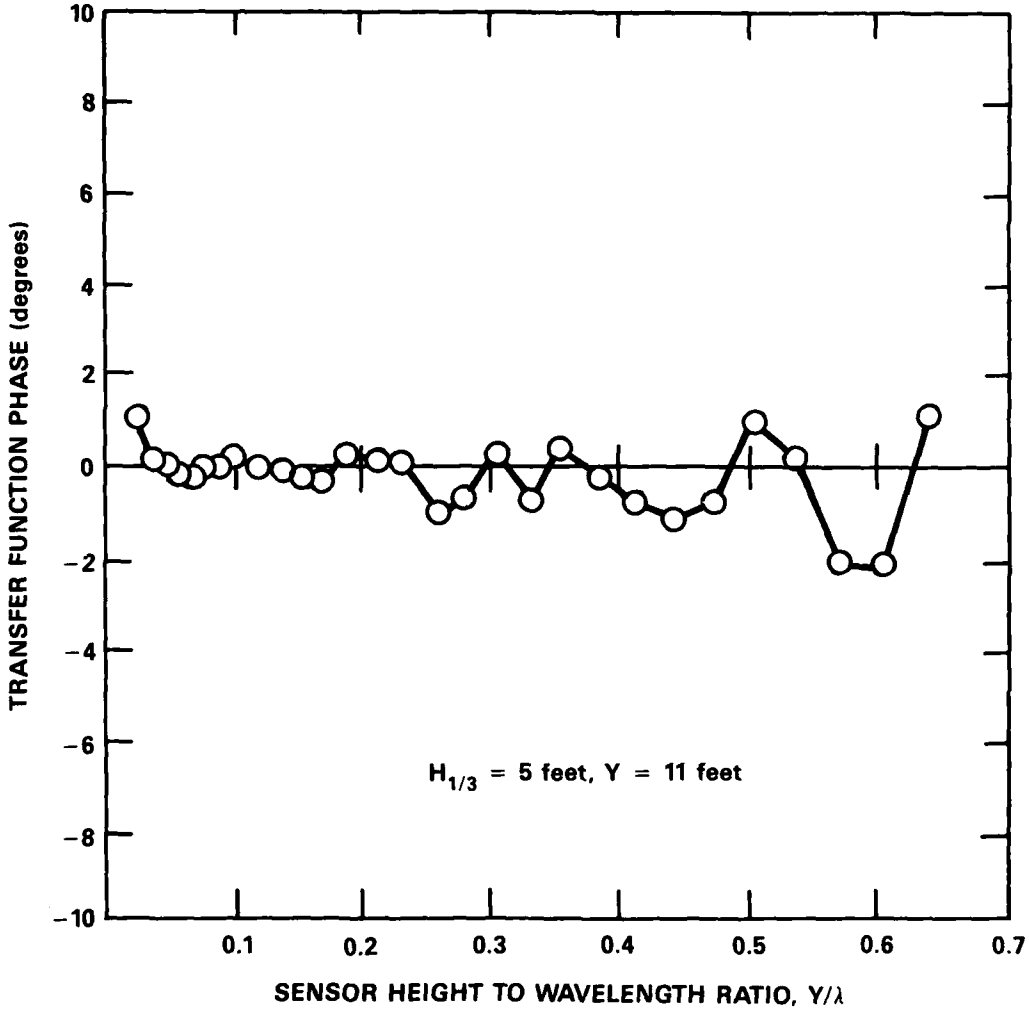

Figure 12 - Transfer Function Phase for Random Wave Profiles

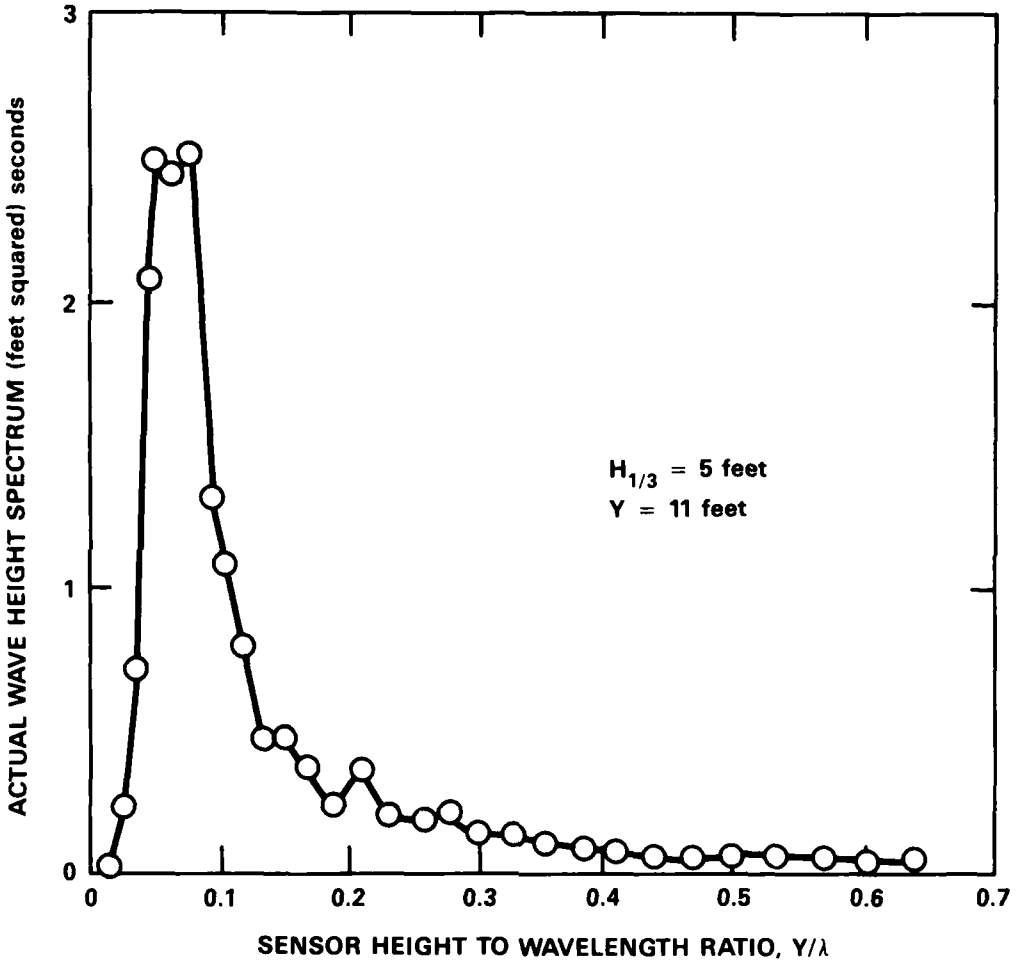

Figure 13 - Auto Spectrum of the Actual Wave Height

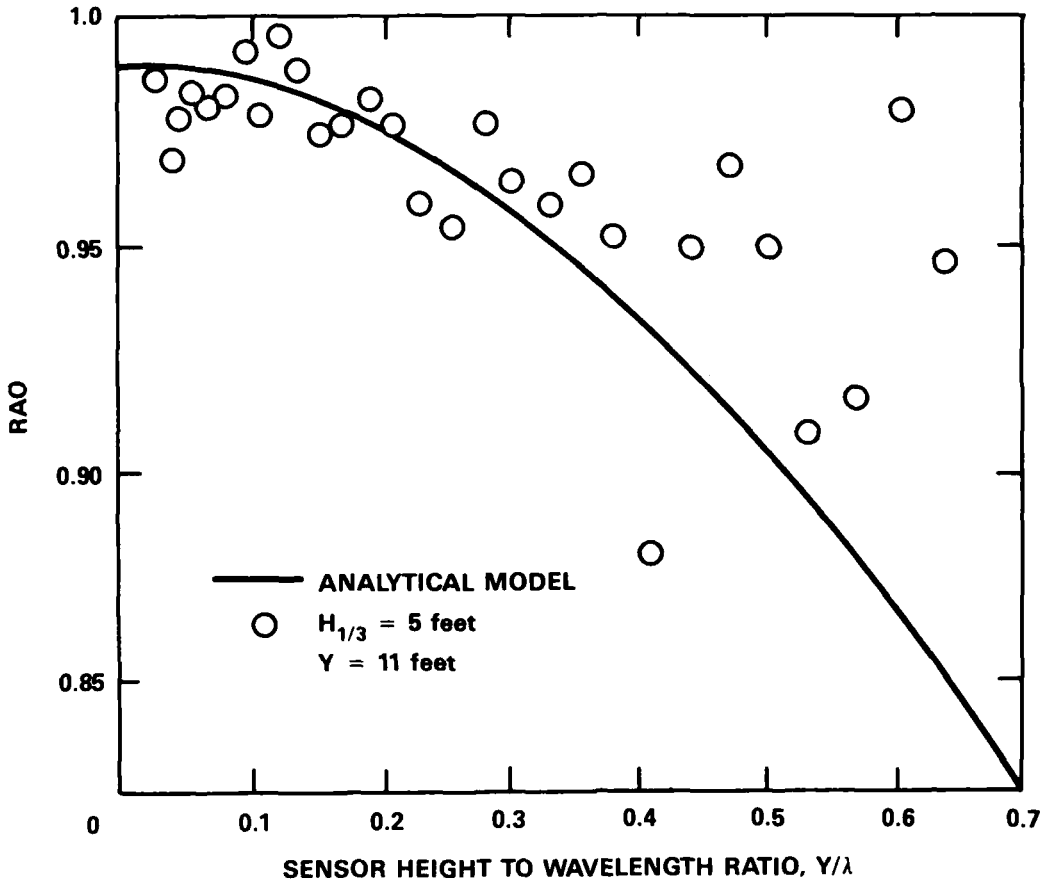

Figure 14 - Response Amplitude Operator, RAO, for the Measured and Actual Wave Height

11-foot sensor height are presented in Figure 15. The coherency predicted by the analytical model is unity for any Y/λ ratio. Beyond Y/λ of 0.35, however, the coherency from the simulation becomes significantly lower than one. This difference is attributed to the neglected quadratic term that affects the measured wave height auto spectrum and RAO at Y/λ ratios greater than 0.35.

8. EXPERIMENTAL MEASUREMENTS OF RANDOM WAVE PROFILES

Experiments were performed in the Maneuvering and Seakeeping facility (MASK) at DTNSRDC where an ultrasonic displacement sensor was used to measure random waves. A surface piercing, capacitance wave height sensor provided a point measurement of the wave height. The comparision of the results from these two sensors demonstrates the ability of the analytical model to predict the off vertical return error in an actual sensor.

8.1. EXPERIMENTAL PROCEDURE AND DATA REDUCTION

The sensor configuration for these experiments included a sonic sensor and a capacitance wave height sensor that served as a standard of comparison and was therefore assumed to be error free. The sonic sensor, a Western Marine Electronics model LM4000, was located 20 inches above the undisturbed water surface. The capacitance sensor was located 14 inches behind and 20.5 inches to the right of the sonic sensor relative to the two dimensional wave crest. The wave maker was about 150 feet foward of these sensors; the sensors were about 12 feet left of center in this 240-foot wide seakeeping basin.

The capacitance wave height sensor served as the reference for wave height in the experiments. The sensitive element is a 3 foot length of Teflon coated wire with an outside diameter of 0.04 inches. One end connects to the electronic signal conditioning circuitry while the other end is water proofed. A 0.02 inch diameter ground return wire is located about 6 inches from the capacitance sensor; this wire extends about 4 feet into the water. The change in capacitance across the wetted length of the Teflon coated wire is converted by the signal conditioning into a voltage signal that is then recorded. The details of this signal conditioning are given in Appendix D.

Time history data were collected from these sensors. Data collection began after the shortest expected wavelengths reached the sensors; the data were collected for about 550 seconds. These data were reduced using methods identical to those

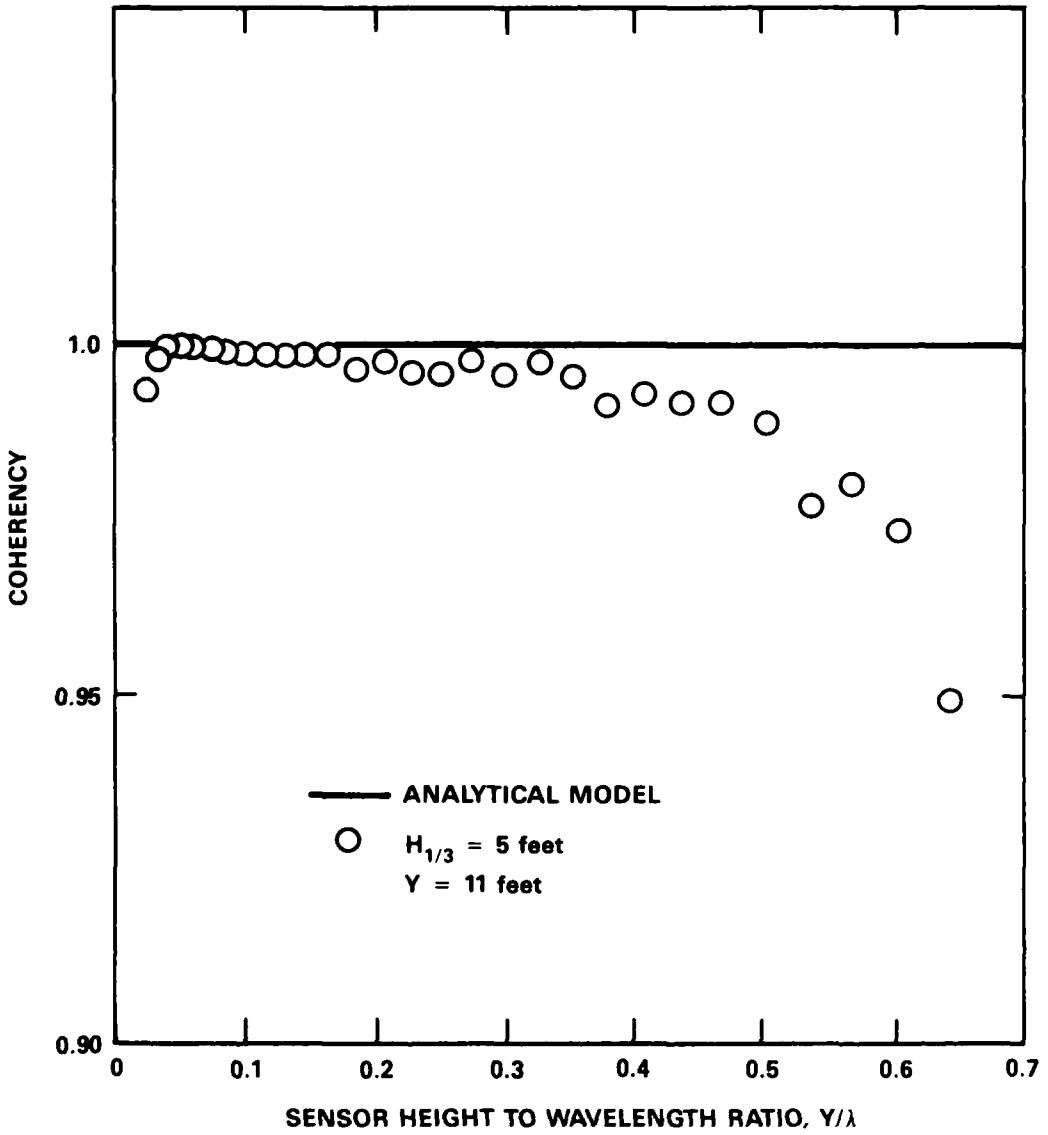

Figure 15 - Coherency for the Measured and Actual Wave Height

applied to the simulated random wave time histories. (See Section 7.2. - Data Reduction of Simulated Data.) For the sonic sensor and the capacitance sensor time histories, these results included estimates of the mean value, standard deviation, auto spectra, cross spectra, coherency and the transfer function. The wave slope variance is estimated from these auto spectra using the numerical integration method described in Appendix C.

8.2. EXPERIMENTAL RESULTS AND COMPARISON TO ANALYTICAL MODEL

The mean value, standard deviation and wave slope variance results for four experimental runs are presented in Table 2. For two of these runs, the auto spectra of the wave height measured by the capacitance probe are presented in Figure 16. The transfer function and coherency between the capacitance and sonic wave height measurements are presented in Figures 17 and 18. For these last two figures, the analytical model results are plotted using the wave slope variance estimates presented in Table 2.

TABLE 2 - MEAN VALUES, STANDARD DEVIATIONS AND WAVE SLOPE VARIANCE FOR EXPERIMENTAL DATA

Parameter	Run 228	Run 229	Run 245	Run 246
Mean Value (inches)				
Sonic	0.1141	0.1721	0.0451	0.0933
Capacitance	0.5147	0.4607	0.5450	0.4834
Standard Deviation (inches)				
Sonic	0.8438	1.578	0.9211	1.573
Capacitance	0.8730	1.576	0.9051	1.583
Wave Slope Variance	0.0038	0.0151	0.0031	0.0137
Relative Sonic Mean (inches)	-0.4006	-0.2886	-0.4999	-0.3901
Mean from Analytical Model (inches)	0.038	0.151	0.031	0.137
Measured Mean Value Shift (inches)	0.112	0.112	0.110	0.110
Mean Shift from Analytical Model (inches)	0.113	0.113	0.106	0.106

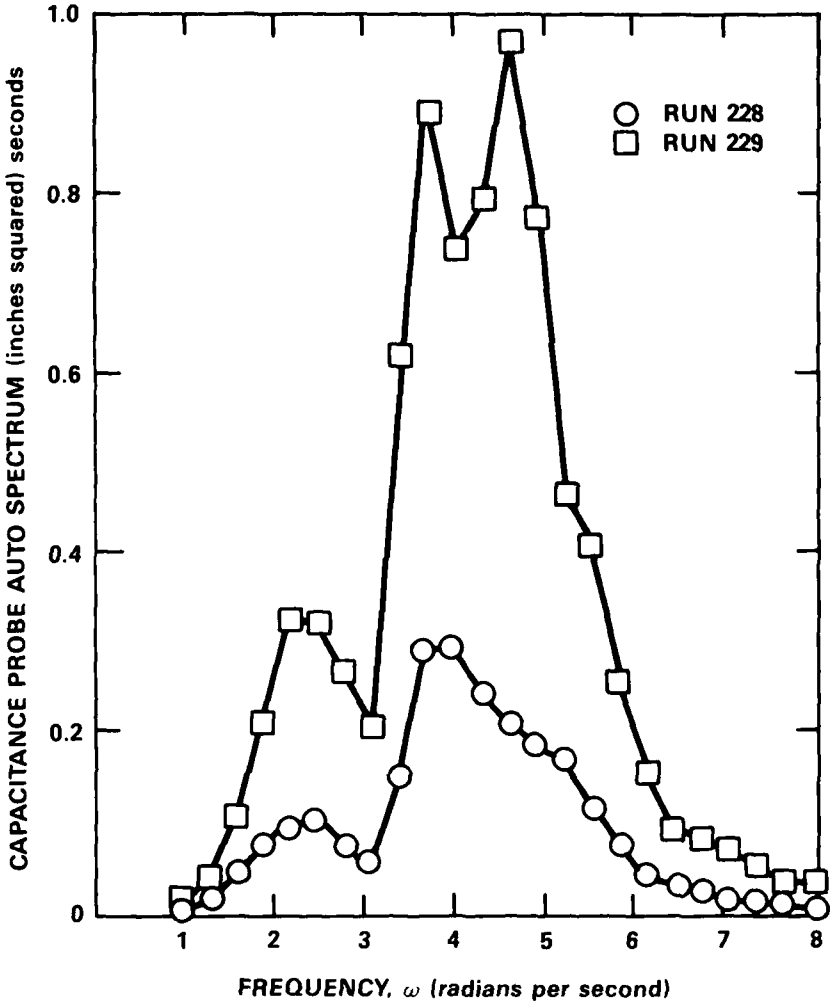

Figure 16 - Capacitance Probe Auto Spectrum for Experimental Runs 228 and 229

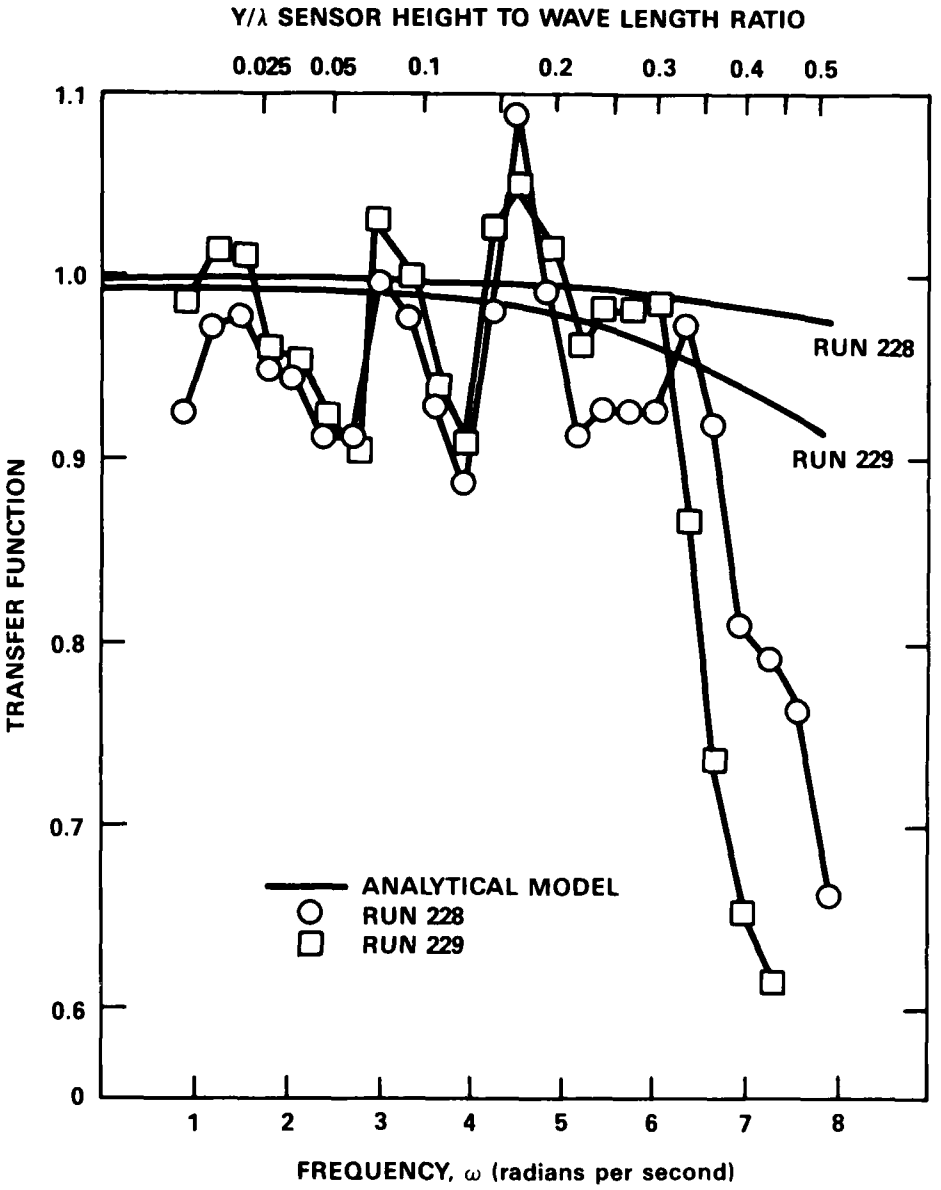

Figure 17 - Linear Transfer Function for Experimental Runs 228 and 229

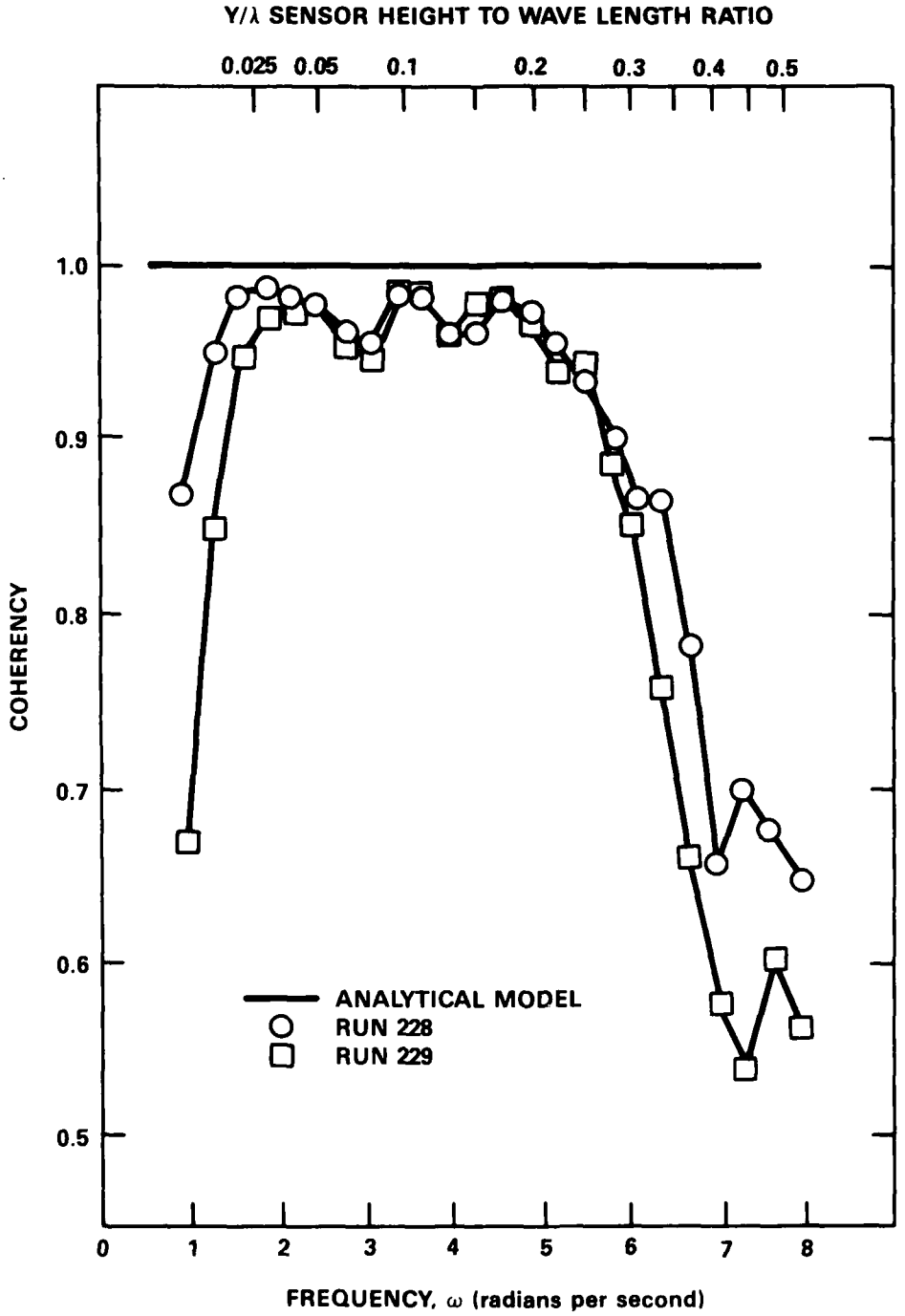

Figure 18 - Coherency Function for Experimental Runs 228 and 229

8.2.1. Mean Value Comparison

Since finite amplitude waves are produced in the test basin, linear wave theory does not strictly hold. Nonlinear effects in the waves will also produce mean value shifts. To remove this uncertainty, the mean value shift of the sonic sensor is measured relative to the capacitance probe's mean value; the capacitance probe's mean value is subtracted from the sonic probe's mean value. These relative sonic mean value results are listed in Table 2 under the heading "Relative Sonic Mean." The mean value shift predicted by the analytical model is calculated and presented in Table 2 under the heading "Mean from Analytical Model." These calculations use the mean bias equation, Equation (58), where the sonic sensor's height above the undisturbed water surface is 20 inches. Since the absolute mean value was not recorded during this experiment, the mean shift is made into a relative shift between two runs; the relative sonic mean shift for one run is subtracted from the other run. The mean value shifts measured by the sonic sensor between runs 228 and 229 and between runs 245 and 246 are listed in Table 2 under the heading "Measured Mean Value Shift." The mean value shift from the analytical model for these same runs is also listed in this table under the heading "Mean Shift from Analytical Model." As seen from the values given in the table, the measured mean value shifts are almost identical to the shifts predicted by the analytical model. This agreement is remarkable in that differences can exist due to drift in the electronic circuitry, and random error or scatter due to finite run lengths.

The measurement of the wave slope variance is occasionally desired for basin tests. The closeness of these mean bias results demonstrate that this aspect of the sonic sensor's error can be utilized for this measurement. One advantage of this method of measuring wave slope variance is that a wave dispersion relationship is not assumed.

8.2.2. Transfer Function Comparison

The transfer function results for runs 228 and 229 are presented in Figure 17. The analytical model results are plotted using Equation (71) with the wave slope variance given in Table 2. In the frequency region above 6 radians per second, both transfer functions rapidly degenerate toward zero. From Figure 16, the wave height auto spectrum is low in this region, and, from Figure 18, the coherency is reducing. These results suggest that background noise in the form of low amplitude, multi-directional waves are beginning to dominate the measurements. These small waves are

generated by the low frequency waves breaking on the wave absorber, the occasional air blown out from the wave maker and waves created by viscous effects along the side of the basin.

In the frequency region from 1 to 6 radians per second, both experimentally derived transfer functions oscillate; a similar oscillation is seen in the coherency. This oscillation is a consistent feature for both runs. The analytical model predictions fall close to but not exactly in the middle of these oscillations. Several factors could cause this shift. Transfer function estimates are biased downward by measurement noise in the input (capacitance sensor in this case) and slight calibration error could exist for either sensor. Another possibility is that the effect producing these oscillations could also cause this shift.

The oscillations occur over a small length scale; the two sensors are separated by about 23 inches. This scale is much smaller than the wave lengths associated with the lower frequencies. Statistically independent phenomena such as waves reflected from the wave absorber could cause spatially oscillating zones of wave intensity; however, they would likely be on the scale of a wavelength. Due to this short length scale, coherent interference patterns is a likely cause of these oscillations. The most likely source of coherent interference patterns is from differences in the wave height produced by different wave maker domes. The same drive signal is controlling each dome; however, the response of each dome can be slightly different.

Regardless of the source of these oscillations in the transfer function, they prevent a complete comparison between the measured transfer function and the transfer function predicted by the analytical model.

9. CONCLUSION

The analytical model is a useful tool for predicting the effects of off vertical return error in ultrasonic displacement sensors. This error can be controlled by proper selection of the height of the ultrasonic displacement sensor above the undisturbed water surface. The mean bias error can be used to measure the wave slope variance.

Specific results include expressions for:

* Linear transfer function magnitude and phase for sinusoidal and random wave profiles.
* Mean value offset or bias for either profile.

* Echo return angle for either profile.
* Amplitude of the second harmonic for the sinusoidal wave profile.

Except for the echo return angle, these expressions are dependent on the sensor height, so the error may be controlled.

REFERENCES

1. Holton, C.E., "Microprocessor Based Dropout Correction for Acoustic Wave Height Gauges," 19th American Towing Tank Conference, Univ. of Michigan, Ann Arbor, Michigan (Jul 1980).

2. Bendat, J.S., Principles and Applications of Random Noise Theory, John Wiley & Sons, Inc., New York, New York (1958).

3. Nuttall, A.H., "Spectral Estimation by Means of Overlapped Fast Fourier Transform Processing of Windowed Data," Naval Underwater Systems Center, Report 4169 (Oct 1971).

4. Welch, P.D., "The Use of Fast Fourier Transforms for the Estimation of Power Spectra: A Method Based on Time Averaging over Short, Modified Periodograms," IEEE Trans. Audio Electroacoustics, Vol. AU-15, pp 70-73 (Jun 1967).

5. Whalen, A.D., Detection of Signals in Noise, Academic Press, New York, New York (1971).

APPENDIX A
SOME PROPERTIES OF GAUSSIAN RANDOM PROCESSES

Since the wave profile is assumed to be a Gaussian random process, some of the general properties of these processes are now described; see Bendat[2] and Whalen[5].

Given p,q,r and s as zero mean, Gaussian random processes (functions of time, t), then:

1. Odd mixed central moments are zero

$$E[pqr] = 0 \tag{A.1}$$

2. The fourth mixed central moment has the form

$$E[pqrs] = E[pq]E[rs] + E[pr]E[qs] + E[ps]E[qr] \tag{A.2}$$

3. Derivatives of Gaussian random processes are also Gaussian.

4. A Gaussian random process and its first derivative are statistically independent

$$E[pp_t] = 0 \tag{A.3}$$

However,

$$E[pp_{tt}] \neq 0 \tag{A.4}$$

in general.

APPENDIX B
SIMULATION OF RANDOM WAVE PROFILE

The wave height at any point in space and time is given by

$$\eta\ (x,t) = \sum_{i=1}^{N} \eta i\ (x,t) \tag{B.1}$$

where N = 50 and

$$\eta_i\ (x,t) = H_i \cos\ (k_i x - \omega_i t) \tag{B.2}$$

The wave number, k_i, is related to wave length, λ_i, in feet by

$$k_i = 2\pi/\lambda_i \tag{B.3}$$

and the frequency, ω_i, is in radians per second. For deep water waves using linear wave theory, the dispersion relationship is

$$k_i = \omega_i^2/g \tag{B.4}$$

where g is the gravitational constant (32.174 feet per second squared). To insure irregularly spaced frequencies for each of the 50 components, the frequency was chosen by

$$\omega_i = 2\pi\ (0.01\ (i-1) + 0.085) + \xi_i \tag{B.5}$$

where ξ_i is a random variable uniformly distributed between +0.031416 to -0.031416 radians per second. The single amplitude height, H_i, in feet was selected to approximate a segment of PM wave spectrum, $G(\omega)$, given by

$$G(\omega) = \frac{0.0081\ g^2}{\omega^5}\ e^{-\frac{33.56}{H_{1/3}^2\ \omega^4}} \tag{B.6}$$

where $H_{1/3}$ is the significant wave height in feet. This amplitude was selected in the following manner.

$$H_i = \sqrt{2\,\sigma_i^2} \tag{B.7}$$

where

$$\sigma_i^2 = \int_{\omega_i - \Delta\omega/2}^{\omega_i + \Delta\omega/2} G(\omega)\, dw \cong G(\omega_i)\, \Delta\omega \tag{B.8}$$

where $\Delta\omega = 0.062832$ radians per second.

APPENDIX C
VARIANCE OF THE WAVE PROFILE'S FIRST AND SECOND SPATIAL DERIVATIVES FOR THE BAND-LIMITED PIERSON-MOSKOWITZ WAVE SPECTRUM

The analytical model requires the variance of the wave profiles first and second derivative. These methods are used to produce the results given in Table 1.

From Equation (63), the wave slope variance, $\sigma^2_{f_x}$, is given by

$$\sigma^2_{f_x} = \frac{1}{g^2} \int_0^\infty \omega^4 \, S(\omega) d\omega \tag{C.1}$$

The band-limited PM wave spectrum is given by

$$S(\omega) = \begin{cases} \dfrac{0.0081 \, g^2}{\omega^5} e^{-\frac{33.56}{H^2_{1/3} \, \omega^4}}, & \omega \leq \omega_o \\ 0, & \text{otherwise} \end{cases} \tag{C.2}$$

where ω_o = 3.613 radians per second. So,

$$\sigma^2_{f_x} = 0.0081 \int_0^{\omega_o} \frac{1}{\omega} e^{-\frac{33.56}{H^2_{1/3} \, \omega^4}} d\omega \tag{C.3}$$

Using the substitution,

$$\nu = \frac{33.56}{H^2_{1/3} \, \omega^4} \tag{C.4}$$

Then,

$$\sigma^2_{f_x} = \frac{0.0081}{4} \left[- E_i \left(- \frac{33.56}{H^2_{1/3} \, \omega_o^4} \right) \right] \tag{C.5}$$

Where $-E_i(-x)$ is the exponential integral

$$-E_i(-x) = \int_x^\infty \frac{e^{-\nu}}{\nu}\, d\nu \tag{C.6}$$

From Equation (99), the variance of the wave profile's second spatial derivative, $\sigma^2_{f_{xx}}$, is given by

$$\sigma^2_{f_{xx}} = \frac{1}{g^4} \int_0^\infty \omega^8\, S(\omega)\, d\omega \tag{C.7}$$

Applying the band-limited PM wave spectrum given by Equation (C.2), then

$$\sigma^2_{f_{xx}} = \frac{0.0081}{g^2} \int_0^{\omega_o} \omega^3\, e^{-\frac{33.56}{H^2_{1/3}\,\omega^4}}\, d\omega \tag{C.8}$$

Again, using the substitution given by Equation (C.4),

$$\sigma^2_{f_{xx}} = \frac{0.0081\ \omega_o^4}{4\ g^2} \left\{ e^{-\frac{33.56}{H^2_{1/3}\,\omega_o^4}} - \frac{33.56}{H^2_{1/3}\,\omega_o^4} \left[-E_i\left(-\frac{33.56}{H^2_{1/3}\,\omega_o^4}\right)\right]\right\} \tag{C.9}$$

The auto spectrum of the actual wave height, $\hat{S}_{ff}(\omega)$, was estimated for each simulation case during data reduction. From these sample auto spectra, the variance of the wave profile's first and second spatial derivatives were estimated using numerical integration

$$\sigma^2_{f_x} = \frac{\Delta_\omega a}{g^2} \sum_{n=1}^{N} \omega_n^4\, S_{ff}(\omega_n) \tag{C.10}$$

and

$$\sigma^2_{f_{xx}} = \frac{\Delta\omega a}{g^4} \sum_{n=1}^{N} \omega_n^8 \hat{S}_{ff}(\omega_n) \qquad (C.11)$$

where $\omega_1 = 0.0$ and $\omega_N = 3.8$ radians per second. ωa is the spacing between spectral estimates.

APPENDIX D
CAPACITANCE WAVE HEIGHT SENSOR

A capacitance wave height sensor was used as a reference for these experiments. The wetted surface of the Teflon coated wire determines the measured water level; the measured capacitance is localized to the Teflon only. This feature reduces spatial biasing in the wave height measurement. Similarly, conductivity changes in the water have little affect on the measurement. This sensor does, however, disturb the water surface. Surface tension effects are present and the characteristics of the surface film change with time. Compared to the shortest wavelengths of interest (3 to 4 feet), the 0.04 inch diameter wire should not significantly affect the wave height measurement. Additional research into these effects is required.

The capacitance wave height sensor used for the basin experiments consists of four sections: a 3 foot section of Teflon coated wire, a ground return wire, signal conditioning electronics and a control box. The Teflon coated wire is water proofed on one end and the signal conditioning electronics are located at the other end. A cable from the control box to the signal conditioning electronics provides power, a control signal and it returns the output from the sensor.

During these experiments, the Teflon coated wire was configured in the following manner. The end beneath the water was tied to 15 feet of monofilament fish leader with a 1 pound weight at the end. This leader forms a pendulum. The natural frequency of this pendulum is about 1.3 radians per second; this frequency is below the lowest frequency expected in the random waves. During the wave runs, only a slight motion was observed; the maximum offset from vertical could not have been more than 0.5 degrees.

The Teflon coated wire and the water form a capacitor; the ground return wire completes this circuit. The fresh water used in the basin has high resistivity, so the equivalent circuit of the sensor is a series connected resistor and capacitor; both circuit elements vary depending on water level. The ground return wire is therefore placed close to the sensor wire (within 6 inches). The signal conditioning method can tolerate moderate levels of this resistance before nonlinearities are observed; however, it can not tolerate capacitance in parallel with the sensor. For this reason, the signal conditioning is located at the top of the sensor. The Teflon coated wire is the no. 26 hook up wire made by Alpha (type number 5853). For this wire, the capacitance will change approximately 5 picofarads per inch of submersion. Teflon has several advantages that make it desirable for this application. Teflon

absorbs 0.01 percent water so its characteristics will change little over prolonged submersion in water. Also, the water scum that accumulates on the wire is easily removed. During the experiment, the wire was cleaned daily.

The circuit for the signal conditioning is given in Figure D.1. A MC14538 CMOS (complementary metal oxide silicon) precision dual one-shot is the major component in this circuit. A one-shot is a digital circuit that, when triggered, produces a state change from zero to one for a fixed time duration. The length of this pulse is controlled by external circuit elements. For the MC14538, this time duration is directly proportional to the product of the resistor and capacitor values attached to its T1 and T2 pins. The linearity of this relationship directly determines the linearity of the wave height sensor. The 2 kilohertz clock signal (+6 to -6 volt square wave) provides the trigger to both one-shots. One one-shot is a reference, while the other is connected to the Teflon coated wire. As the water level varies, the time duration of its pulse will vary proportionally. The reference one-shot provides compensation for any drift that affects both one-shots. Inside the MC14538, both one-shots are on the same silicon chip, so any temperature variations should affect both one-shots the same way. The output signal from the control box is a voltage that is proportional to the time duration difference between both one-shots. Two outputs are provided from each one-shot, Q and $\overline{Q}$. When the Q output goes from -6 to +6 volts, the $\overline{Q}$ output goes from +6 to -6 volts. The Q_S output from the water level sensing one-shot and the $\overline{Q}_R$ output from the reference one-shot are sent over the cable to the control box. At the control box, these two signals are added. As seen in Figure D.2, a nonzero sum results only for the time duration difference of the two one-shots. This differential measurement cancels equivalent effects such as temperature drift.

The control box contains power supplies, the clock oscillator and the summing circuit for the Q_S and $\overline{Q}_R$ outputs. Once this sum is formed, the voltage pulses are averaged by a resistor/capacitor filter. This filter rejects most of the 2 kilohertz clock signal, and it passes the frequencies contained in the wave height. In the experiment, the output from the control box was filtered again by a six pole, Butterworth filter with a -3 decibel frequency of 6 hertz.

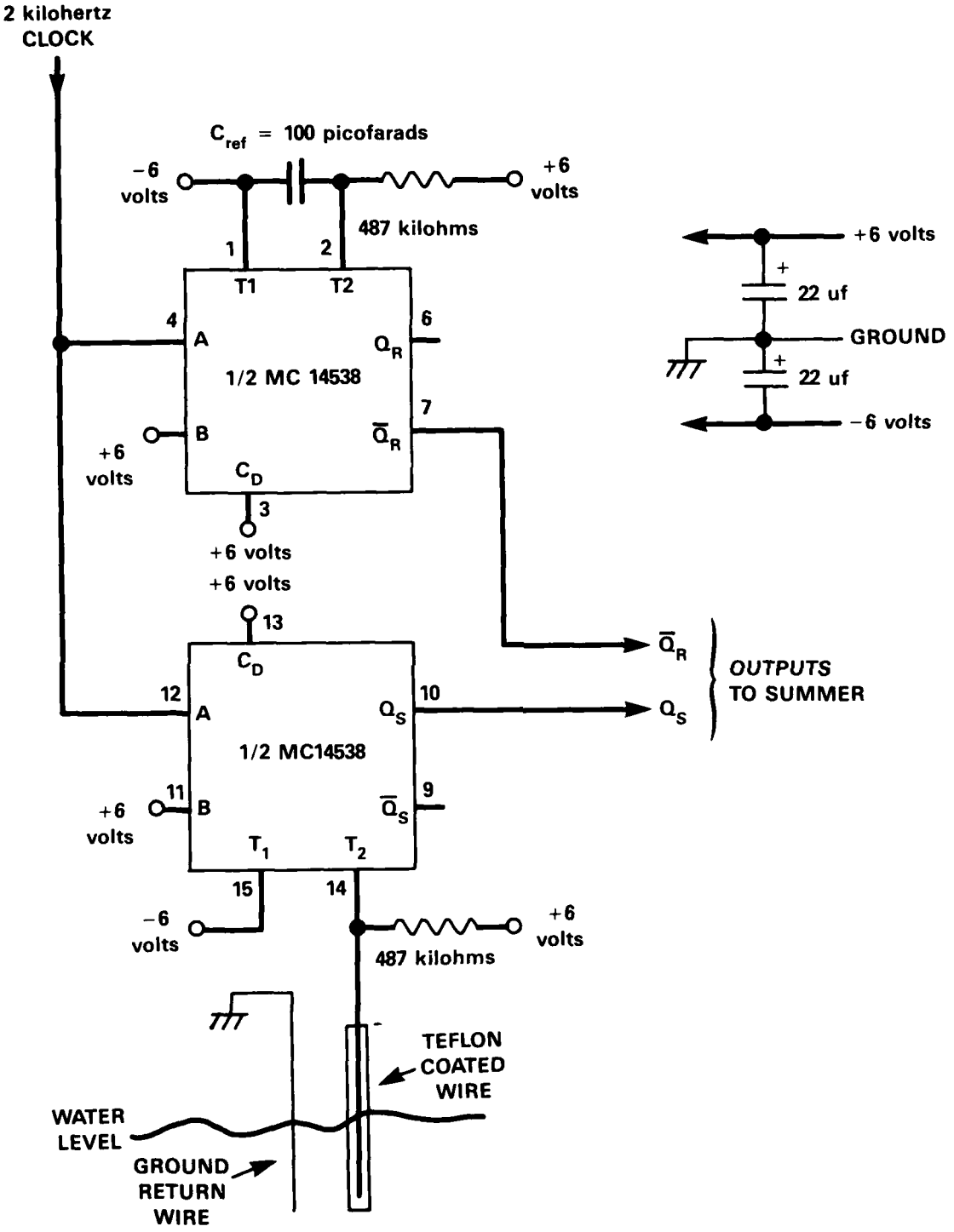

Figure D.1 - Circuit Diagram for Capacitance Sensor's Signal Conditioning

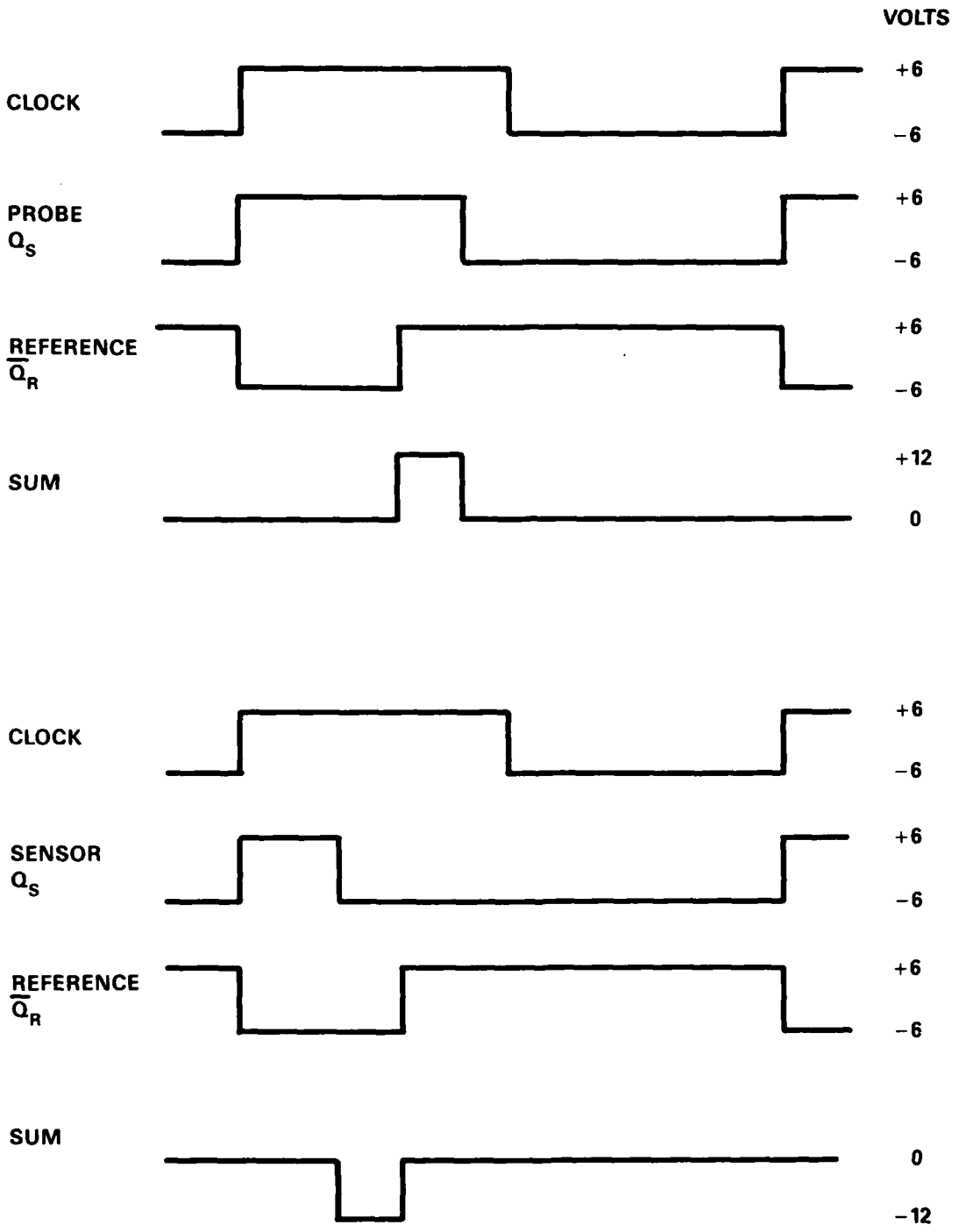

Figure D.2 - Timing Diagram for One-shots in Capacitance Sensor's Signal Conditioning

INITIAL DISTRIBUTION

Copies	
12	DTIC
1	City College of New York W.J. Pierson
1	University of California W. Webster
1	University of Florida M.K. Ochi
1	University of Michigan A. Troesch
1	M.I.T. M. Abkowitz

Copies	Code	Name
1	2900	G.G. Switzer
1	2950	R.T. Schwartz
10	2960	R.D. Pierce
10	5211.1	Reports Control
1	522.1	TIC (C)
1	522.2	TIC (A)

CENTER DISTRIBUTION

Copies	Code	Name
1	012.3	D.D. Moran
1	1200	W.G. Dietz
1	1204	W.M. Richardson
1	1221	Z.G. Wachnik
1	1500	W.B. Morgan
1	1504	V.J. Monacella
1	1522	M.B. Wilson
1	1560	D.S. Cieslowski
1	1561	G.G. Cox
5	1561	J.F. O'Dea
1	1561	S.L. Bales
1	1562	M.J. Davis
1	1563	J.E. Russ
1	1600	H.R. Chaplin
1	1630	A.G. Ford
1	1730.6	W.H. Buckley

DTNSRDC ISSUES THREE TYPES OF REPORTS:

1. **DTNSRDC reports, a formal series,** contain information of permanent technical value. They carry a consecutive numerical identification regardless of their classification or the originating department.

2. **Departmental reports, a semiformal series,** contain information of a preliminary, temporary, or proprietary nature or of limited interest or significance. They carry a departmental alphanumerical identification.

3. **Technical memoranda, an informal series,** contain technical documentation of limited use and interest. They are primarily working papers intended for internal use. They carry an identifying number which indicates their type and the numerical code of the originating department. Any distribution outside DTNSRDC must be approved by the head of the originating department on a case-by-case basis.

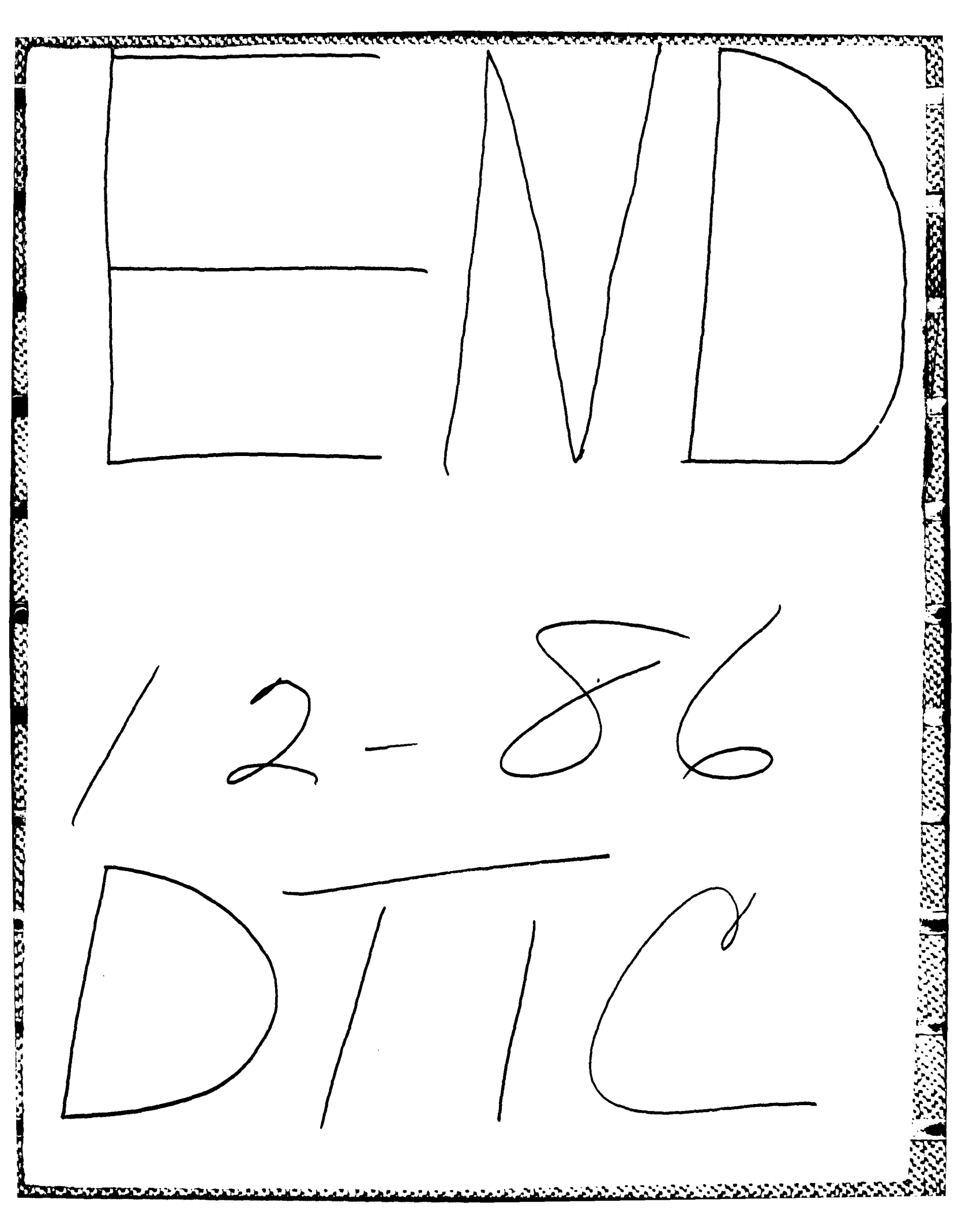
END
12-86
DTIC